Hindawi Publishing Corporation
Advances in Materials Science and Engineering
Volume 2015, Article ID 209286, 18 pages
http://dx.doi.org/10.1155/2015/209286

Research Article

Effect of Cu Addition on the Electrochemical Corrosion Performance of Ni_3Al in 1.0 M H_2SO_4

J. Porcayo-Calderon,[1] R. A. Rodriguez-Diaz,[1,2] E. Porcayo-Palafox,[1] J. Colin,[3] A. Molina-Ocampo,[1] and L. Martinez-Gomez[4,5]

[1]*Universidad Autonoma del Estado de Morelos, CIICAp, Avenida Universidad 1001, 62209 Cuernavaca, MOR, Mexico*
[2]*Universidad Politécnica del Estado de Morelos, Boulevard Cuauhnáhuac 566, 62550 Jiutepec, MOR, Mexico*
[3]*Universidad Autonoma del Estado de Morelos, Facultad de Ciencias Químicas e Ingeniería, Avenida Universidad 1001, 62209 Cuernavaca, MOR, Mexico*
[4]*Universidad Nacional Autonoma de Mexico, Instituto de Ciencias Físicas, Avenida Universidad s/n, 62210 Cuernavaca, MOR, Mexico*
[5]*Corrosión y Protección (CyP), Buffon 46, 11590 Mexico City, DF, Mexico*

Correspondence should be addressed to J. Porcayo-Calderon; jporcayoc@gmail.com

Received 2 March 2015; Revised 22 May 2015; Accepted 28 May 2015

Academic Editor: Daniel Guay

The effect of Cu addition on the electrochemical corrosion behavior of Ni_3Al intermetallic alloy was investigated by potentiodynamic polarization, open-circuit potential, linear polarization resistance, and electrochemical impedance spectroscopy in 1.0 M H_2SO_4 solution. Performance of the pure elements (Cu, Ni, and Al) was also evaluated. In general, Cu addition improved the corrosion resistance of Ni_3Al. Electrochemical measurements show that corrosion resistance of Ni_3Al-1Cu alloy is lower than that of other intermetallic alloys and pure elements (Ni, Cu, and Al) in 1.0 M H_2SO_4 solution at 25°C. Surface analysis showed that the Ni_3Al alloys are attacked mainly through the dendritic phases, and Cu addition suppresses the density of dendritic phases.

1. Introduction

Acid solutions are extensively utilized in the industry sector for several purposes, such as acid pickling, industrial acid cleaning, acid descaling, and oil well acidizing [1]. The corrosion behavior of carbon steel in acidic solution is significant considering its widespread applications, namely, in the manufactures of pipe lines for petroleum industries. Acid solutions are frequently used in the removal of rust and scale-developed in industrial process. Since the steel is the major structural material utilized in the construction industry, there have been considerable efforts focused on the prevention of steel corrosion. As most steels are stable in neutral or alkaline media, acidic environments are the major concern. However, a group of materials that could serve as substitutes of steel are the intermetallics compounds when exposed to acidic solutions because these compounds possess good corrosion and oxidation resistance in media, containing not only oxygen but also sulphur, good abrasion resistance, and small density. Particularly, many researchers have reported the beneficial effects of the addition of noble elements for inhibiting the anodic and cathodic reactions of the steel immersed in a corrosive environment [2–5]. In low alloy steels the addition of copper plays a major role in the improvement of corrosion resistance [6]. However, in order to transport and store acids solutions like H_2SO_4, it is important to select properly the materials suited for these processes [7].

The ordered intermetallic alloys based on aluminides of transition metals like Fe, Ni, Nb, Ti, and Co are among the materials that can perform properly in industrial processes exposed to acid solutions since the aluminum concentration of these compounds contributes to the formation of a passive layer of aluminum oxide, which is responsible for the good

oxidation, corrosion, and sulfidation resistance at room temperature or higher; besides these intermetallic compounds retain strength and stiffness at elevated temperatures [8, 9]. In particular nickel aluminides based on Ni_3Al and NiAl are expected to be promising structural materials due to their high melting point, low density, and high specific modulus [10, 11] However major drawbacks of these materials are the low ambient temperature ductility, poor fracture toughness, and inadequate elevated temperature strength, which prevent these materials from being used for practical applications. It has been reported that macroalloying NiAl intermetallic compound with Cu and Fe, ductility as high as 6% and 12% can be achieved [12]. It has also been reported that the addition of elements like Cu, Co, Ti, and Fe can improve the mechanical properties of Ni-Al intermetallics [13–15].

Additionally, numerous alloys based upon Ni_3Al have been developed with broad applications ranging from furnace rolls and radiant burner tubes for steel production to heat treating fixtures, forging dies, and corrosion-resistant parts for chemical industries [16, 17]. This is due to the strong bonding between Al and Ni, which remains at elevated temperatures, which produces excellent properties competitive with those of superalloys and ceramics, such as high melting point, low densities, high strength, and good corrosion and oxidation resistance [16–19]. Ni-Al type intermetallics are widely used due to their high temperature oxidation resistance and their ability to develop an Al_2O_3 protective layer which also provides corrosion resistance in molten salts [20, 21].

Despite the fact that nickel aluminides are of interest for high temperature applications, various room temperature applications are being discovered, for example, biomaterials, and seawater atmosphere applications also [22–24]. Some other uses are in fossil plants, where stainless steels, among other materials, are commonly used [25, 26]. Low temperature corrosion performance of Ni-Al compounds is of interest for high temperature applications because these materials will not perpetually be at operating temperatures, since transients like start-ups and shutdowns in fossil plants can occur. In these plants, sulfur is present and, in these transients, condensation of H_2SO_4 takes place producing the so-called "dew point corrosion" which could lead to catastrophic failures during service. Therefore, the main objective of this work is to investigate the effect of the Cu addition on the corrosion performance of the Ni_3Al intermetallic alloy in sulfuric acid at low temperature.

2. Experimental Procedure

2.1. Materials. Cast ingots of binary Ni-25 at.% Al and ternary Ni25Al-xCu (x = 1, 3, and 5 at.%) alloys were produced in quartz crucibles with an induction furnace in an inert atmosphere from elements of 99.99% purity. Ingots were cooled and subsequently solidified inside the crucibles in the furnace at room temperature and in this condition were used in the studies.

2.2. Sample Preparation. The test specimens were cut into small parallelepiped pieces of 5.0 × 5.0 × 3.0 mm using a diamond tipped blade. For electrical connection, specimens were spot-welded to a Ni20Cr wire and then mounted and encapsulated in thermosetting resin. Sample surfaces were ground to 600 grade grit paper and then first rinsed with distilled water and later by ethanol in an ultrasonic bath for 10 minutes. Specimens with this surface condition were employed as the working electrode (WE) in the electrochemical tests.

2.3. Electrochemical Measurements. The electrochemical performance of the intermetallic alloys was determined by open-circuit potential (OCP), polarization curves (PC), linear polarization resistance (LPR), and electrochemical impedance spectroscopy (EIS) measurements. The potentiodynamic tests were performed by means of an Interface 1000 Gamry Potentiostat/Galvanostat/ZRA analyzer. A saturated calomel electrode (SCE) and a platinum wire were employed as a reference and as a counter-electrode, respectively. All the potentials described in the text are relative to the SCE, unless stated differently. In order to evaluate the effect of the Cu addition on the corrosion performance of the Ni_3Al, the intermetallic alloys were exposed in a solution of 1.0 M H_2SO_4 at 25°C for 48 hours.

PC were carried out by polarizing the samples in the potential range of −300 to 1000 mV at 1 mV/s from rest potential (E_{corr}). Prior to the test, the system was allowed to stabilize for 30 min. Corrosion current density, i_{corr}, cathodic and anodic Tafel slopes, and the corrosion potential, E_{corr}, were calculated using the Tafel extrapolation method in the scanned potential ±250 mV from E_{corr}. Also the OCP as a function of time of the working electrodes was measured. The polarization resistance, R_p, was obtained from LPR curves by polarizing the working electrodes from −20 to 20 mV, from E_{corr}, at 1 mV/s scan rate according to ASTM G59-97. From the LPR curves, the slope of the linearly fitted E versus I data was considered as R_p. The corrosion rates were calculated in terms of the corrosion current, i_{corr}, using the Stern-Geary equation [27]:

$$i_{corr} = \frac{b_a b_c}{2.303 R_p \left(b_a + b_c\right)}, \quad (1)$$

where R_p is the polarization resistance and b_a and b_c are the Tafel slopes.

EIS measurements were recorded under open-circuit conditions using a sinusoidal excitation voltage of ±10 mV, and frequencies ranged from 100,000 to 0.01 Hz. After testing, corroded specimens were analyzed in a DSM 960 Carl Zeiss scanning electronic microscope (SEM). The corrosion behavior of the Ni, Cu, and Al was also evaluated as a baseline.

3. Results and Discussion

3.1. Potentiodynamic Polarization Curves. Polarization curves for unalloyed Ni_3Al and ternary Ni_3Al with additions of 1, 3, and 5 at.% of Cu are shown in Figure 1(a). Figure 1(b) shows a zoom at the zone where the electrochemical parameters were determined. The polarization curves for binary and ternary alloys present an active-passive behavior. All alloys exhibit a wide passivation zone. Increasing the Cu

Table 1: Electrochemical parameters of the tested materials in a 1.0 M H_2SO_4 solution at 25°C.

Material	E_{corr} (mV)	b_a (mV/Dec)	b_c (mV/Dec)	i_{corr} (μA/cm^2)	$^*E_{pp}$ (mV)	$^*i_{pp}$ (μA/cm^2)	$^*E_{rp}$ (mV)	$^*i_{rp}$ (mA/cm^2)
Ni_3Al	−279	40	124	9.1 ± 0.05	−105	15000 ± 0.05	—	—
Ni_3Al-1Cu	−279	49	90	2.8 ± 0.05	104	17000 ± 0.05	—	—
Ni_3Al-3Cu	−272	65	140	3.8 ± 0.05	190	55000 ± 0.05	—	—
Ni_3Al-5Cu	−249	90	157	4.5 ± 0.05	73	15000 ± 0.05	164 ± 0.00005	18
Ni	−297	71	122	31.2 ± 0.05	−70	16000 ± 0.05	498 ± 0.00005	450 ± 0.00005
Cu	−121	81	437	2.5 ± 0.05	—	—	—	—
Al	−682	274	136	56.0 ± 0.05	—	—	—	—

$^*E_{pp}$ and i_{pp} indicate the primary passivation potential and primary passivation current density.
$^*E_{rp}$ and i_{rp} indicate the repassivation potential and current density, respectively.

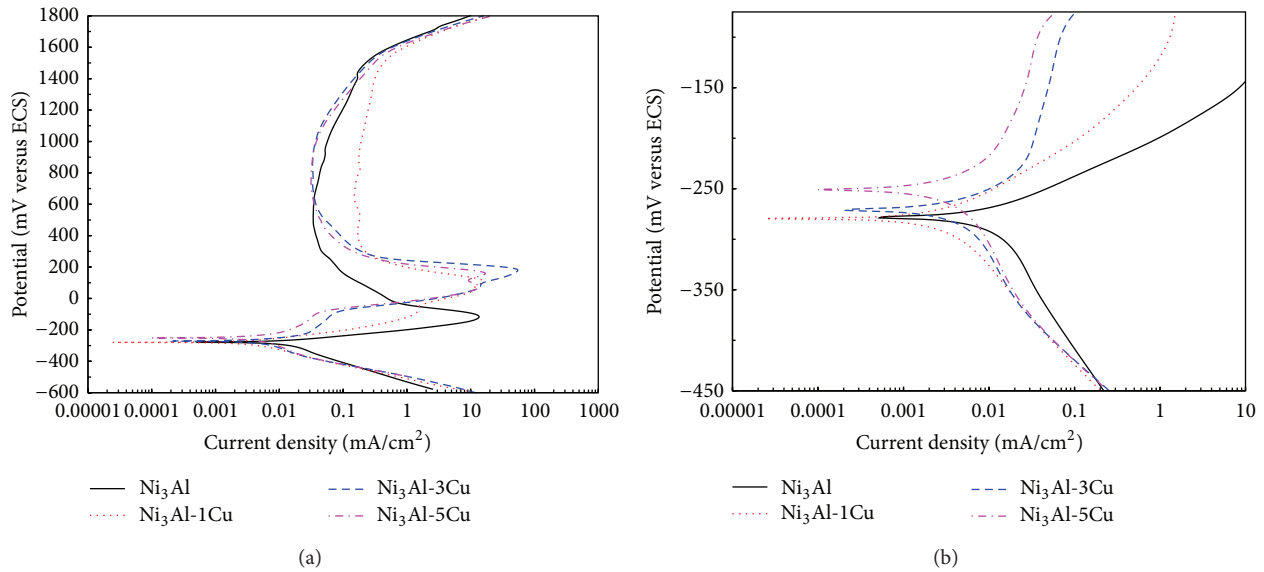

Figure 1: Polarization curves of the Ni_3Al-xCu intermetallic compounds tested in a 1.0 M H_2SO_4 solution at 25°C.

addition to the Ni_3Al alloy induced a shift of E_{corr} towards positive direction of ordinate axis, which means that the E_{corr} value turned nobler under these circumstances.

According to Table 1, the corrosion current density, i_{corr}, values of the ternary Ni_3Al-xCu alloys were lower than those of the binary alloy Ni_3Al which presented an i_{corr} of 9.1 μA/cm^2. This means that the Cu addition to Ni_3Al induced a beneficial effect since the corrosion rate of alloy was diminished. However, as the Cu addition was increased from 1 to 5 at.%, the corrosion current density of ternary alloy was increased from 0.0028 to 0.0045 mA/cm^2. In a similar research, the effect of Cu addition on the corrosion behavior of NiAl intermetallic exposed to 0.5 M H_2SO_4 solution was studied [28], and the authors reported an E_{corr} value of −110 mV together with an i_{corr} equal to 0.02 μA/cm^2 in the NiAl intermetallic alloy. Thus the minor corrosion current density of NiAl as compared with that of Ni_3Al studied in the present work probably is due to the different concentration of H_2SO_4 and to the higher Al content of NiAl which promotes the formation of the passive aluminum oxide film in a higher content on surface of intermetallic. Also, the Cu addition to NiAl intermetallic induced a decrease on its corrosion rate expressed in terms of corrosion current density. Thus, the effect of adding Cu to the Ni_3Al intermetallic on its corrosion rate is in agreement with previous investigations. A similar effect of the enhancement of corrosion resistance as a consequence of Cu addition has also been observed in steels as was described in Introduction. For example, Pardo et al. [29] studied the influence of cementation and electrodeposition of copper coatings on the corrosion resistance of AISI 304 stainless steel immersed in 30 wt.% H_2SO_4 at temperatures of 25 and 50°C. The authors stated that the improved corrosion resistance is related to copper dissolution at the initial stages of exposure tests and the presence of Cu^{2+} in the solution, which makes the medium more oxidizing, increasing in this way the stability of the passive layer. In addition, the presence of copper at the surface reduces the overpotential of cathodic reaction, enabling the transition from an active region to a passive one. From Table 1, it can be seen that the primary passivation potential, E_{pp}, of the binary Ni_3Al alloy was

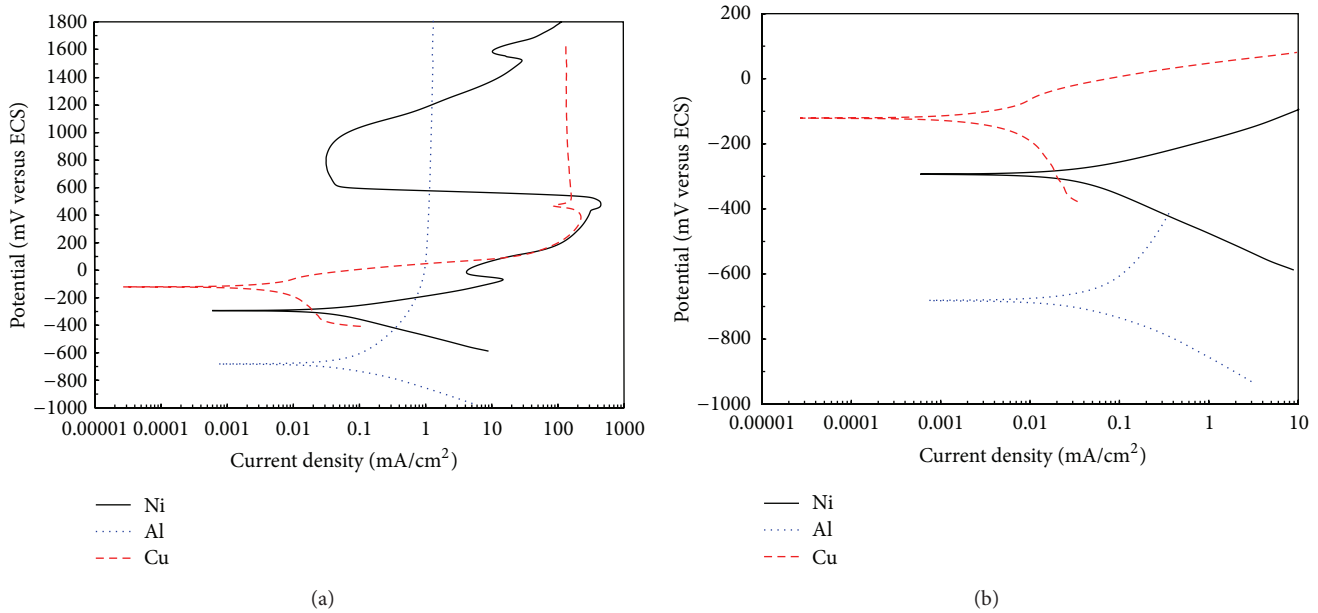

FIGURE 2: Polarization curves of Ni, Cu, and Al tested in a 1.0 M H_2SO_4 solution at 25°C.

minor than that of ternary Ni_3Al-xCu alloys. This indicates that the binary intermetallic compound begins its passivation at minor overpotentials with respect to corrosion potential, E_{corr}. So, in this case, the addition of Cu shifted the E_{pp} towards nobler values. According to Figure 2, the metal Ni exhibited a primary passivation and repassivation, whose E_{pp} and E_{rp} values are presented in Table 1. The polarization curve of the metal Ni exhibited a wide repassivation zone. So, in this case as content of Ni in the Ni_3Al alloy is present in a higher concentration, the passivation process remains in the binary and ternary intermetallics, where this repassivation behavior of the ternary Ni_3Al-xCu alloys could be associated with the adsorption of species such as $CuSO_4{\cdot}5H_2O$, Cu_2O, or $Cu_x(OH)_y$ and similar compounds of Ni.

In order to understand the role of Al, Ni, and Cu in the corrosion behavior of the present aluminides, polarization curves of pure Ni, Al, and Cu elements are shown in Figure 2(a). Figure 2(b) shows a zoom at the zone where the electrochemical parameters were determined. From this illustration it can be observed that the noblest corrosion potential, E_{corr}, corresponded to Cu, while Al element exhibited the most active corrosion potential with E_{corr} equal to −682 mV. The minor corrosion rate in terms of corrosion current density corresponded to pure Cu with an i_{corr} value of 2.5 μA/cm^2. So, in this case as the copper presented the minor corrosion rate, it seems that this element induced a diminution of the corrosion current density values of Ni_3Al-xCu alloys. Moretti and Guidi [30] carried out potentiodynamic polarization tests of Cu exposed to a 0.5 M aerated H_2SO_4 solution at 20°C and 30°C. The authors reported corrosion current densities of 0.0137 and 0.0161 mA/cm^2. After comparing these values of current densities with the ones measured in this work, it can be inferred that the increment of H_2SO_4 concentration does not seem to induce an increment in corrosion rate of pure Cu. Bastidas et al. [31] performed potentiodynamic polarization tests in Cu exposed to various concentrations of sulfuric acid from 0.001 to 1.0 M H_2SO_4 at 25°C. The authors reported that, at low sulfuric acid concentration, the copper dissolution is the main process, while for the highest H_2SO_4 concentration (1.0 M), a passivation phenomenon may take place on the copper surface, yielding the lowest corrosion rate. In previous investigations, the copper passivation phenomenon originated by the exposure to H_2SO_4 acid at a concentration of 1.0 M has been attributed to the formation of $CuSO_4{\cdot}5H_2O$ and/or Cu_2O [32]. So, the passivation phenomenon observed in the present work in the intermetallic Ni_3Al-xCu compounds and in the pure Cu is certainly due to the formation of a passive film formed by copper oxide or copper sulphate on their surfaces, as is explained in the previous research [32]. The passivation behavior observed in the present work was also observed in a previous research where the electrochemical behavior of copper electrode in concentrated sulfuric acid solutions was studied. In this research the passive film was constituted by an inner layer of a mixture of copper oxides and an outer layer of copper sulphate hydrate [33]. Also, the passivation process observed in the present work in pure Cu and in the ternary Ni_3Al-xCu alloys could be related to the oxidation of Cu to Cu(I) and Cu(II) species, as was reported by Hurtado et al. who performed electrochemical studies of Cu-Ni alloy exposed to 0.5 M H_2SO_4 solution [34]; the authors reported that the anodic current is associated with the oxidation of metallic copper to interfacial Cu(I) and Cu(II) species.

The anodic current density of pure Al increased with increasing potential, but at around 100 mV the increase of current density tended to reach a kind of anodic limit current density; this behavior is ascribed to the passive aluminum oxide film that is formed on its surface, as is well known.

Thus, when Ni is alloyed with Al, the passive aluminum oxide film remains on surface of the intermetallic Ni_3Al. This passivation phenomenon is evident by looking at the polarization curves displayed in Figure 1, where a wide passivation zone is observed when the binary and ternary intermetallic compounds are exposed to H_2SO_4. The Cu metal exhibits a first passive zone within the small interval of potentials from 400 to 480 mV, but after 500 mV a kind of anodic limit current density is observed. This behavior is similar to that reported by Arukalam et al. who reported a spontaneous passivation process above 250 mV for copper immersed in 0.5 M sulfuric acid [35]. The polarization curve of Ni exhibited an active-passive-transpassive behavior. In this case a first small passivation zone started at a passivation current, I_{pass}, near to 15 mA/cm^2 and at passivation potential of about −85 mV. Also, for Ni, a second bigger passivation zone started at a potential of 500 mV. Besides, the corrosion potential, E_{corr}, of pure Ni was equal to −297 mV with its corresponding corrosion current density, i_{corr}, equal to 31.2 μA/cm^2. Additionally, pure nickel displayed an anodic Tafel slope of 71 mV/decade. The anodic Tafel slope determined for the pure Ni in the present work is in agreement with the reported one by Amin et al. [36], who studied the inhibition of corrosion of Ni exposed to 1.0 M H_2SO_4 solution; the authors observed that, for the Ni electrode without inhibitor, a linear relation was observed between potential E and $\log(i)$ in the active dissolution region, with an apparent anodic Tafel slope of 67 mV/decade. It is worth noting that the chemical composition of passive films is very important in defining the corrosion resistance [37]. Table 1 shows the electrochemical parameters obtained from polarization curves.

3.2. Open-Circuit Potential Measurements. The change of the E_{corr} value with time for the different alloys together with Ni, Al, and Cu which were tested during 48 h in a solution of 1.0 M H_2SO_4 is presented in Figure 3. In the first moments of immersion, the rest potential of each electrode moves towards less negative values due to the initial formation and growth of the passive oxide film. In all cases after the initial rise in the rest potential, a certain constant potential value (steady-state potential) is attained.

In this plot, it can be observed that the Cu additions alloy turned the E_{corr} value of the Ni_3Al alloy towards more noble values for up to 200 mV. In other words, the steady-state rest potential (i.e., E_{corr}) became more positive with the increase in Cu content (except for 1 at.% Cu). In addition, the slope of the linear rise in the rest potential (dE/dt) for intermetallic alloys, which is a measure for the passivation rate [38], increases according to the following order: Ni_3Al < Ni_3Al-5Cu < Ni_3Al-3Cu < Ni_3Al-1Cu. These findings revealed that the tested alloys tend to passivate in H_2SO_4 solution, and the rate of passivation depends on Cu concentration. This behavior indicates a more active corrosion surface of binary Ni_3Al alloy when compared with ternary Ni_3Al-xCu alloys; also this comportment is in agreement with the highest corrosion rate exhibited by the binary Ni_3Al alloy (Table 1). In this case, the passivation phenomenon could be attributed to the formation of $CuSO_4{\cdot}5H_2O$ and/or Cu_2O protective phases. However, the addition of 1 at.% Cu did not change in a significant way

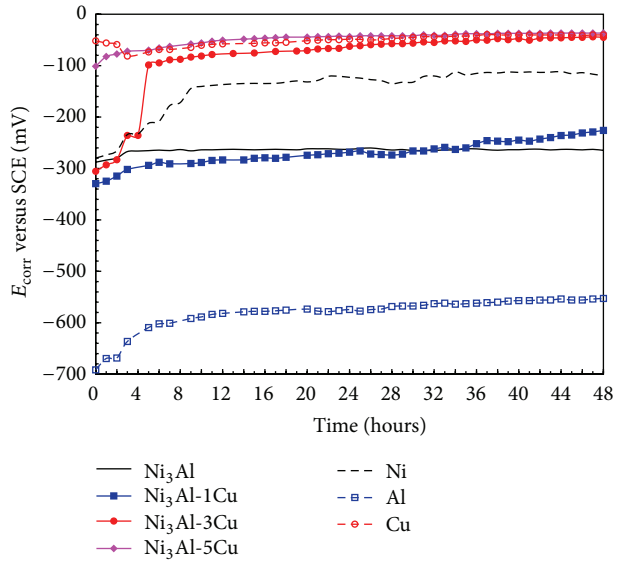

FIGURE 3: Variation of E_{corr} values for the tested materials in a 1.0 M H_2SO_4 solution as a function of exposure time.

the E_{corr} value of the Ni_3Al intermetallic alloy during the whole exposure time, while for the pure elements (Al, Ni, and Cu), the more active E_{corr} value was observed in Al with a mean E_{corr} value near to −580 mV. This illustration shows that the noblest E_{corr} among the pure elements corresponded to Cu, while Al displays the more active corrosion potential. In this case, the most active corrosion potential and the highest corrosion current density was exhibited by Al, which could be attributed to the low corrosion resistance of the Al-oxide layer formed on the aluminum surface, but when the Al and Ni form the intermetallic Ni_3Al compound, then the aluminum oxide film formed on the intermetallic surface probably is more compact and less porous, and the passivity of this layer is enhanced by its modification with Ni-oxide. The fact that the E_{corr} value of pure Cu is the noblest during the whole exposure time is in agreement with the corrosion potential values determined from the polarization curves; see Figure 1. Besides, copper addition caused a shift of the E_{corr} value towards nobler potentials during the 48 h of immersion. Thus, when the Cu was added to the Ni_3Al alloy, the nobility of Cu induced an improvement of the passivation process on surface of the ternary Ni_3Al-xCu alloy, where this effect is probably due to the modification of the aluminum oxide layer by the copper oxide or sulphate. The initial decrease of the E_{corr} value observed in copper could be explained and related to a previous research [34] where the authors studied the electrochemical behavior of the annealed Cu-5 wt.% Ni alloy in 0.5 M H_2SO_4 solution. The investigators reported that, immediately after immersion, the OCP measurements of Cu exhibited an initial diminution from the initial value and reached a steady state after 5 h of exposure in the aerated and deaerated solution. In this case, the observed decrease of potential is explained in terms of the dissolution of the naturally formed copper oxide film, followed by the oxidation of the metal to form Cu(II) species.

Ni showed an initial increase of its OCP value; afterward the OCP value reached a more or less steady state after the 10 hours of immersion. This behavior is in agreement with a previous research [34], where the authors reported that, for Ni in the aerated electrolyte, the OCP increases monotonically, from the initial immersion potential towards a more or less steady-state value. This indicates that, in 0.5 M H_2SO_4 solution, the Ni is oxidized to form a passive layer. The investigators also established that the steady state was attained in a relatively short time (3 h) in the aerated solution. In the deaerated solution, however, the steady state was not attained, even after 15 h. Because steady state was reached faster in the aerated solution, this process depended on the concentration of dissolved oxygen and therefore it can be inferred that it is controlled by the cathodic reduction of oxygen.

According to curves shown in Figure 3, the more anodic potentials of the Cu-containing specimens suggest that the presence of Cu influences the kinetics of the anodic reaction by shifting the E_{corr} values toward nobler values. This behavior is in agreement with the reported one by Oguzie et al. [37] who investigated the effect of Cu addition on the electrochemical corrosion behavior of stainless steels in both the active and passive states in 0.1 M H_2SO_4 solution. The authors reported that the Cu addition generally improved the corrosion resistance and facilitated the passivation phenomenon but did not notably affect the resistance of the passive films. Generally, the effect of alloying of copper on the corrosion of nickel/copper alloys is manifested by an increase in nobility of the corrosion potential, a widening of the active-passive transition range, an increase in critical and passive current densities, and a contraction of the passive zone [39].

3.3. Corrosion Current Measurements. The variation of corrosion rate in terms of the corrosion current density as a function of exposure time for Ni_3Al alloys and pure Cu, Ni, and Al elements in 1.0 M H_2SO_4 solution is displayed in Figure 4. It can be seen that, for pure elements, the Al element exhibited the highest corrosion rate while the Ni presented the minor corrosion rate for the 48 h of exposure. Regarding pure Cu metal, the i_{corr} of this element exhibited a trend to increase as the exposure time had elapsed. This behavior could be attributed to the good stability of the passive film and its growth on the copper surface. Therefore, the addition of Cu to the aluminide, Ni_3Al, induced stability on its surface film by the modification of the aluminum oxide. Also, from the same illustration, it can be observed that the addition of 1% Cu to Ni_3Al alloy induced a diminution of corrosion rate in the intermetallic compound after 16 hours of exposure. Conversely, the additions of 3% and 5% Cu to Ni_3Al induced an increase of the corrosion rate up to about 0.01 mA/cm^2 in the intermetallic compound. The minor corrosion rate of Ni_3Al-1Cu as compared with the other intermetallic compounds is consistent with the corrosion current density values determined by the polarization curves; see Figure 1. Besides, the corrosion rate of Ni_3Al-3Cu and Ni_3Al-5Cu remained more or less stable during the whole immersion time, while that of the Ni_3Al-1Cu intermetallic tended to diminish after the 30 hours of exposure in the acidic media, which means that the passive film was very stable

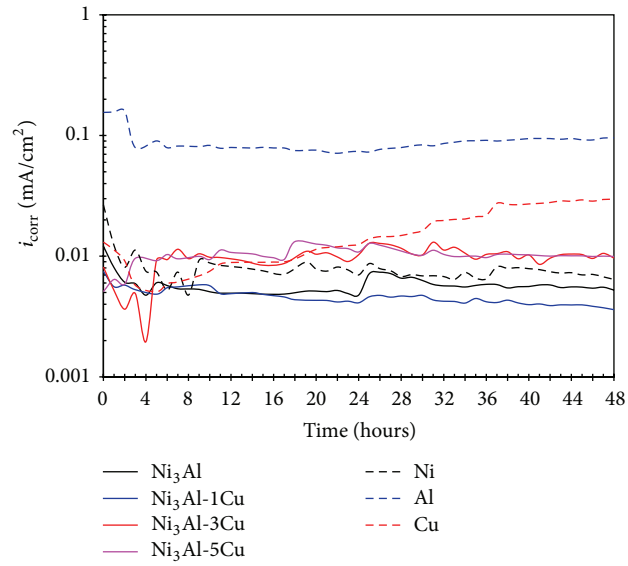

FIGURE 4: Variation of i_{corr} values for the tested materials in a 1.0 M H_2SO_4 solution as a function of exposure time.

when the Ni_3Al intermetallic compound was alloyed with 3 and 5% of Cu.

3.4. Electrochemical Impedance Spectroscopy. Bode plots for the metals and intermetallic alloys exposed to 1.0 M H_2SO_4 solution at 25°C are shown in Figures 5–11. Analysis from Bode diagram is simpler because it minimizes the dispersion of the experimental data and shows a finer description of the frequency-dependent behavior of the electrochemical data, where these features are not observed in the Nyquist diagrams. From the Bode diagram the following basic elements can also be identified in order to establish the configuration of the equivalent circuits describing the electrochemical system [40]; resistors (R) that appear as plateaus, and in this case $|Z| = R$ and $\phi \to 0°$, capacitors (C), where $|Z|$ is a straight line with a −1 slope and $\phi \to 90°$, and elements associated with diffusion, where $|Z|$ has a −0.5 slope and $\phi = 45°$. In general, three frequency regions referring to the high, intermediate, and low frequency values are obtained from Bode diagrams [41, 42].

Figure 5 shows the Bode plot for Ni. Ideally, at higher frequency region ($f > 1000$ Hz), the Bode plot exhibits a plateau (horizontal line) of the $|Z|$ values with the phase angle approaching 0°, and this is the response of the solution resistance, R_s. However, in the Bode plot for Ni, the plateau is observed at frequencies higher than 10 kHz. This could be due to the presence of a film either porous or slimy onto Ni surface. In the middle frequency region (1000 to 10 Hz), an ideal spectrum displays the maximum phase angle approaching −90° and a linear slope of about −1 in $\log|Z|$ as $\log(f)$ decreases, and this is the characteristic response of capacitive behavior of the electrode and describes the dielectric properties of the electronically conducting surface film. It is known that a phase angle greater than or equal to 90° signifies that the protective layer is an effective insulating film; hence

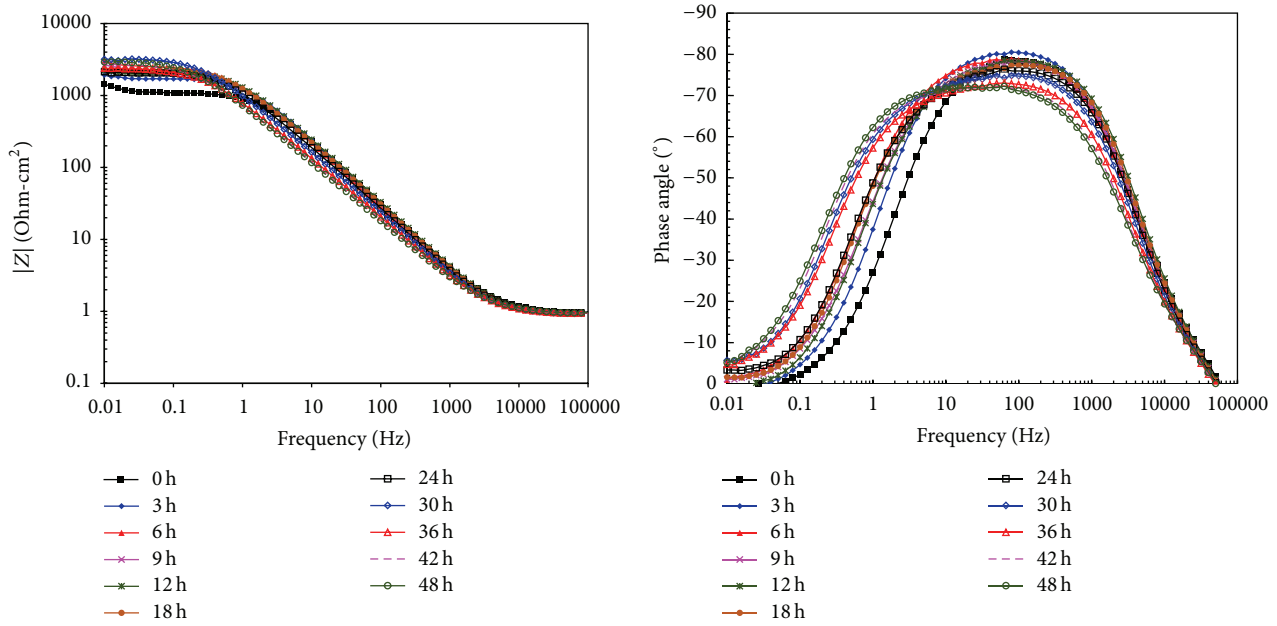

Figure 5: Bode plots for nickel in 1.0 M H_2SO_4 solution at 25°C.

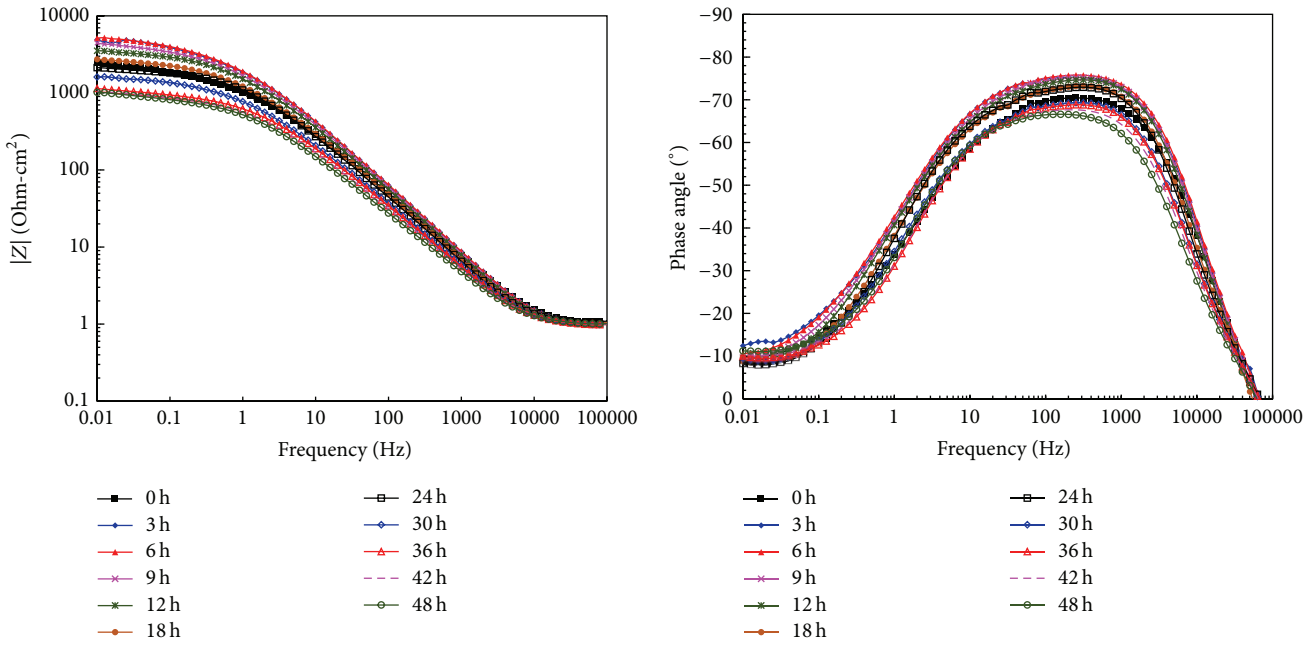

Figure 6: Bode plots for copper in 1.0 M H_2SO_4 solution at 25°C.

there is no current leakage at defect sites, but if the phase angle is less than 90°, then the protective layer is permeable to ions from solution [43]. In this case, the formation of two maxima phase angles is observed. At time 0 hours, a maximum phase angle (80°) is observed at 100 Hz, and, as time elapses, a new maximum phase angle at lower frequencies is observed (3 Hz). Both time constants showed similar values of phase angle (70°). This can be associated with the presence of two protective layers, one of them (a film either porous or slimy) in contact with the electrolyte and the other one (oxide film) in contact with the Ni. Generally, at low frequency region ($f < 10$ Hz), the Bode plot exhibits a plateau (horizontal line) of the $|Z|$ values with the phase angle approaching 0°, and in this region the electron charge transfer process, the mass transfer processes, or other relaxation processes taking place at the film-electrolyte interface or within the pores of the surface film are detected. However, in this case, these features are observed at lower frequencies than 0.1 Hz. $|Z|$ values show an increase in the early hours of immersion to later show oscillating values. This may be associated with

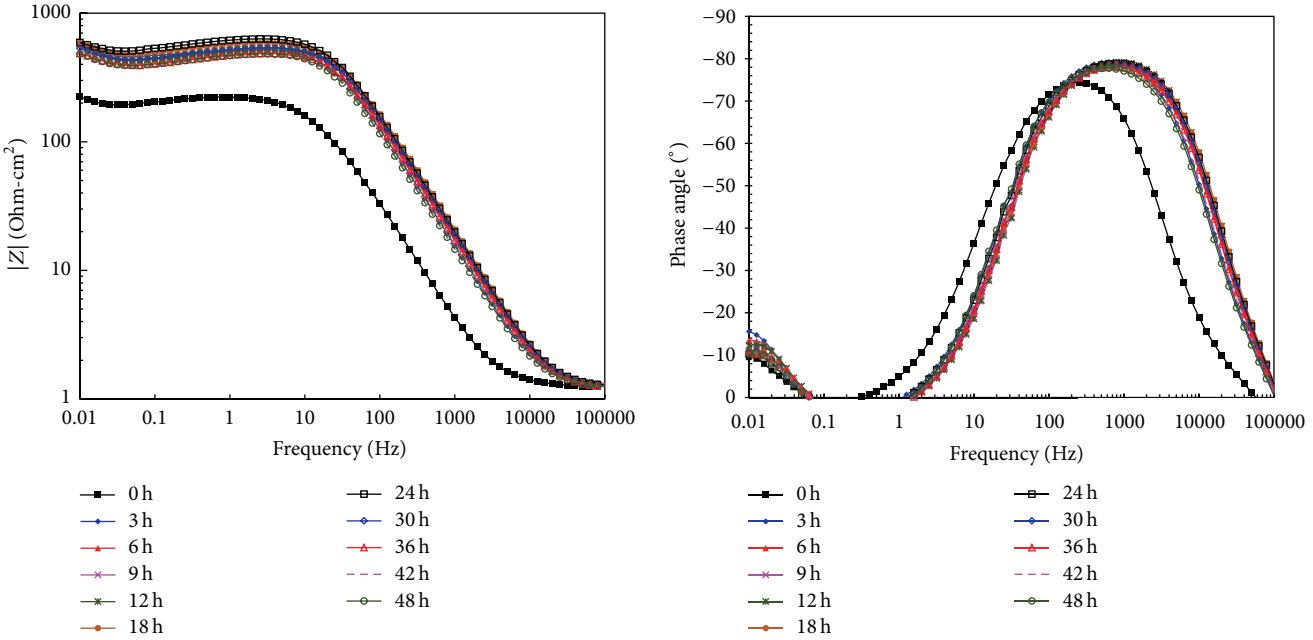

Figure 7: Bode plots for aluminum in 1.0 M H_2SO_4 solution at 25°C.

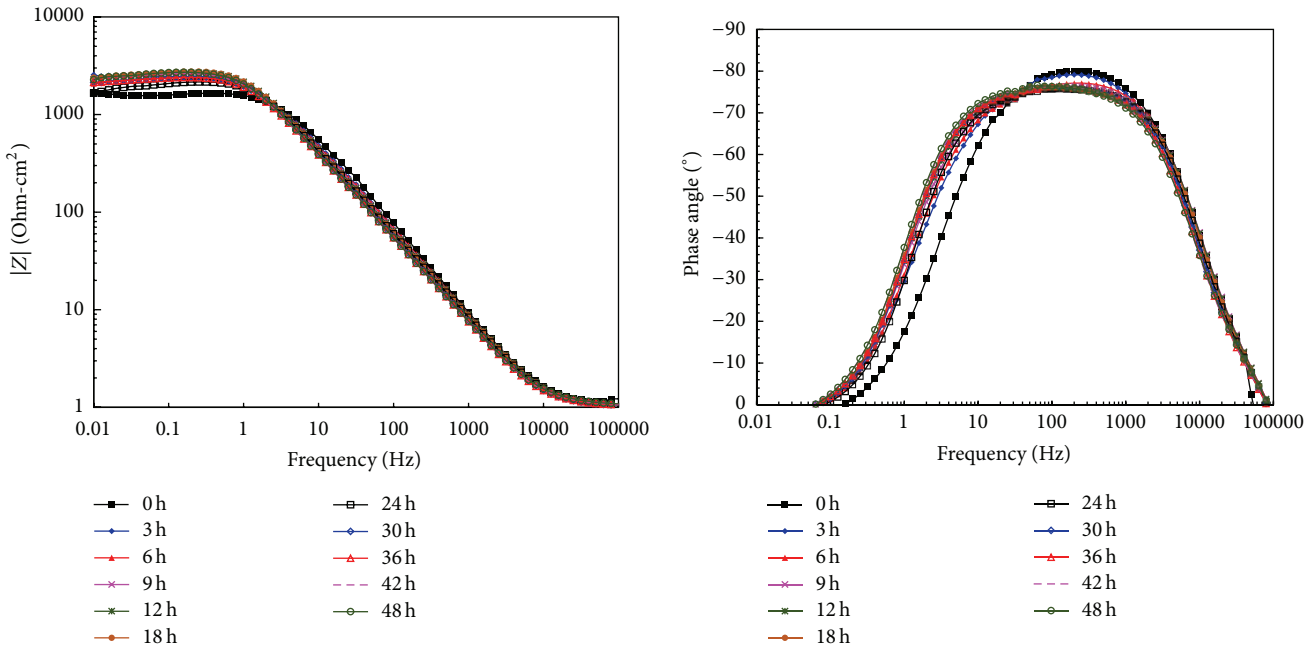

Figure 8: Bode plots for Ni_3Al in 1.0 M H_2SO_4 solution at 25°C.

processes of dissolution and regeneration of the surface layers. These results were consistent with the Nyquist diagram (not shown), where it could be observed that the data described a depressed, capacitive-like semicircle, with its center at the real axis, indicating that the corrosion process is under charge transfer control from the metal surface to the solution through the double electrochemical layer, and, as time elapsed, the semicircle diameter increased but after 6 hours the semicircle diameter decreases and increases constantly. This behavior is consistent with that observed in LPR measurements.

Generally, the anodic dissolution of Ni in acid solutions involves uniform dissolution with the following reaction path (which considers the water adsorption process in the mechanism of electrooxidation) [36, 42]:

$$Ni + H_2O \longleftrightarrow NiOH + H^+ + e^- \quad (2)$$

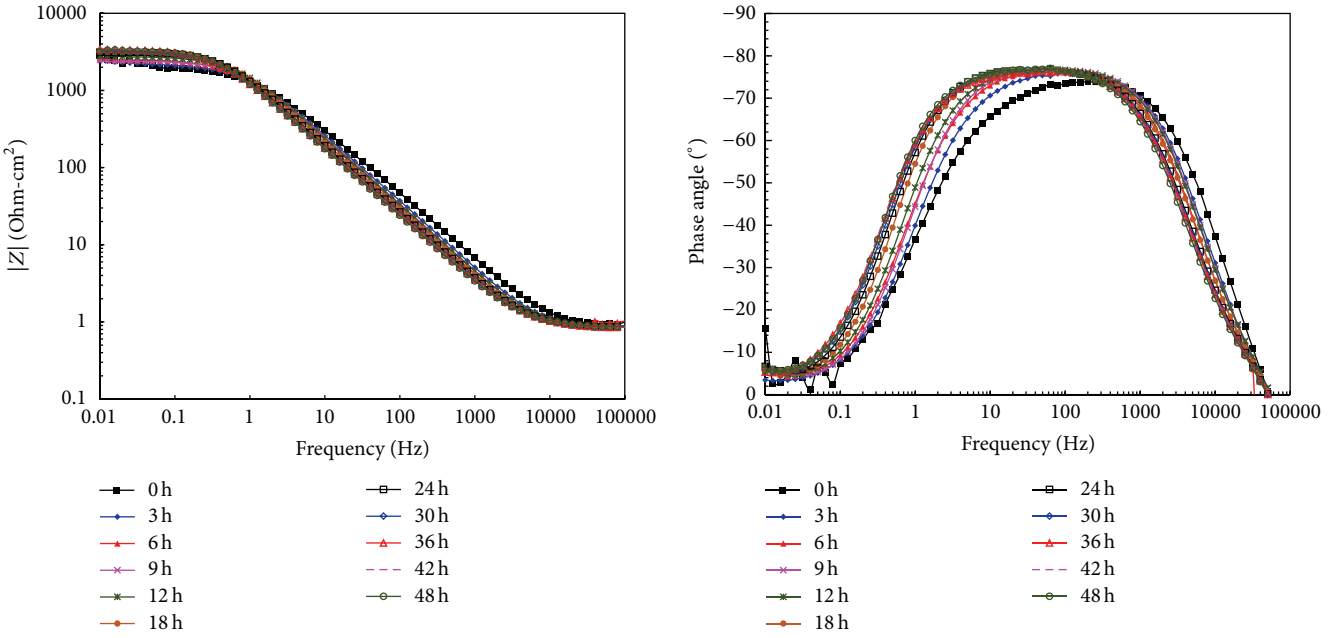

Figure 9: Bode plots for Ni_3Al-1Cu in 1.0 M H_2SO_4 solution at 25°C.

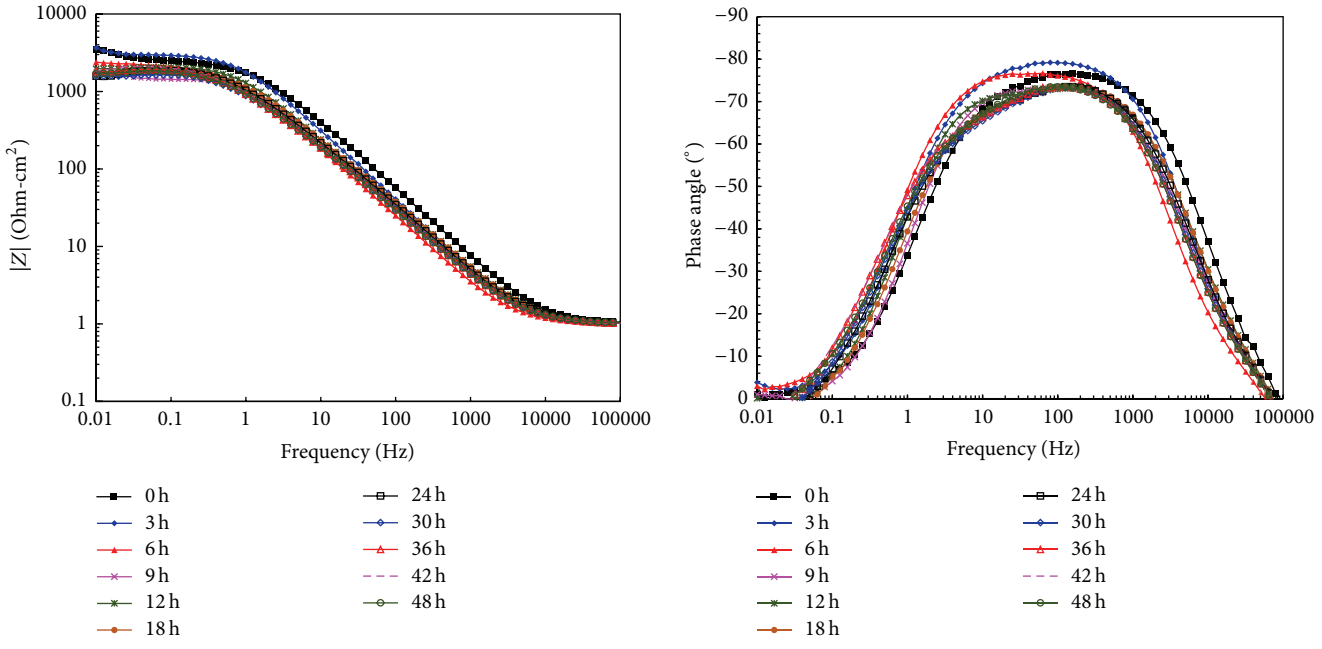

Figure 10: Bode plots for Ni_3Al-3Cu in 1.0 M H_2SO_4 solution at 25°C.

$$NiOH + H^+ \longleftrightarrow Ni^+ + H_2O \quad (3)$$

$$Ni^+ \longleftrightarrow Ni^{2+} + e^- \quad (4)$$

where the cathodic reaction is the reduction of H_3O^+, occurring on the electrode surface:

$$2H_3O^+ + 2e^- \longleftrightarrow 2H_2O + H_2 \quad (5)$$

However, it also has been suggested that the passivating film formed on a nickel electrode in acid solutions is formed by $Ni(OH)_2$, NiO, NiOOH, or NiOOH intermediates [39]. This suggests that the time constant observed in high-middle frequency can be a hydroxy-derivative of Ni which is adhered to the metallic surface, and the time constant at low frequencies corresponds to a thin film of NiO.

Figure 12(a) shows the superficial aspect of Ni after the corrosion test in 1.0 M H_2SO_4 solution at 25°C. After the corrosion test, the working electrodes used were washed gently with distilled water and ethanol before analysis by SEM.

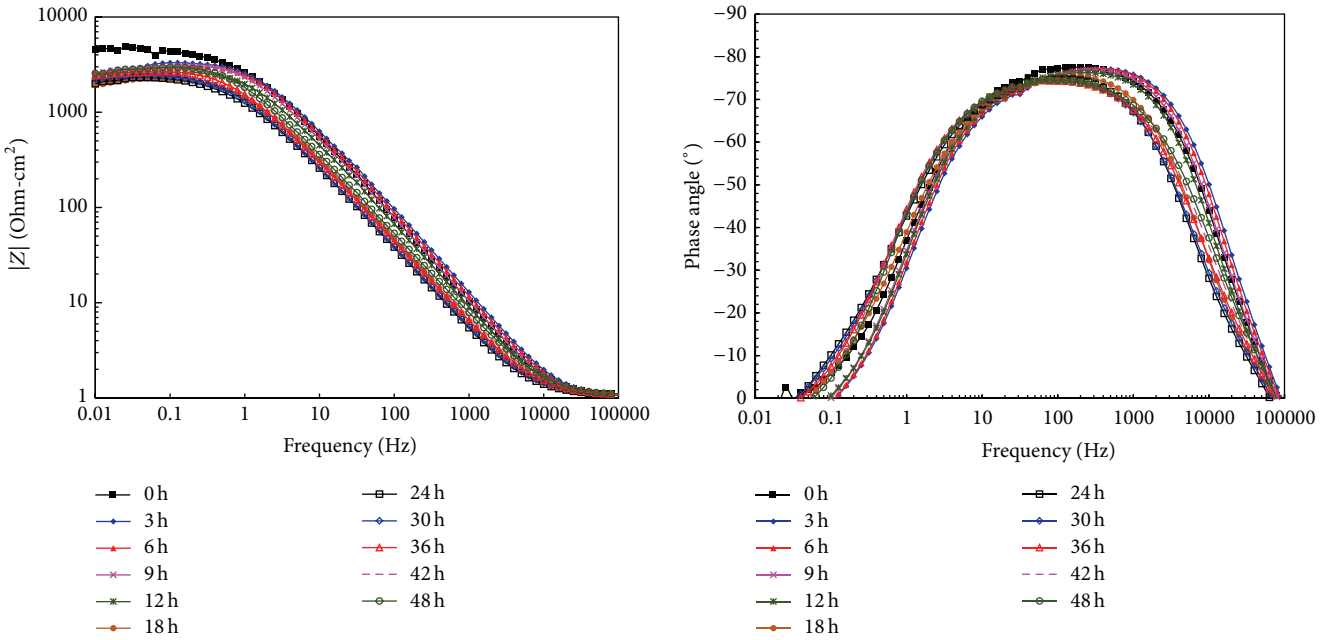

Figure 11: Bode plots for Ni_3Al-5Cu in 1.0 M H_2SO_4 solution at 25°C.

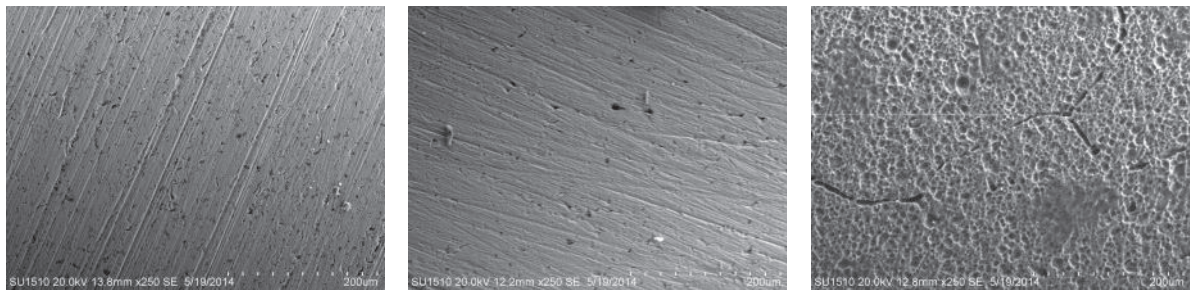

(a) Nickel (b) Copper (c) Aluminum

Figure 12: Micrograph of the corroded surfaces of (a) nickel, (b) copper, and (c) aluminum in 1.0 M H_2SO_4 solution at 25°C.

During the surface inspection, the presence of corrosion products onto the metallic surfaces was not detected, indicating that these were soluble and they were dissolved during the washing step of the working electrodes. The Ni surface did not show a significant attack, since the presence of lines generated by the grinding process is still observed. The superficial attack undergone by the Ni corresponds to that defined as uniform corrosion.

Figure 6 shows the Bode plot for Cu. Cu behavior is very similar to that observed behavior with Ni. At higher frequency region ($f > 1000$ Hz), the plateau of the $|Z|$ values with the phase angle approaching 0° is observed at frequencies higher than 10 kHz. Again, this could be due to the presence of a film either porous or slimy onto Cu surface. In the middle frequency region (1000 to 10 Hz), a maximum in the phase angle is observed. However, the shape of the phase angle spectrum is not according to a Gaussian distribution. The width of the spectrum is located from the high frequency region to the low frequency region. This suggests the presence of two time constants. As time evolved, phase angle increases from 70° to 76° and after 6 hours decreases (66°) until the end of the test. This is associated with an increase in the slope of the relationship log f-$|Z|$ and a subsequent decrease. This can be due to the presence of two protective layers, one of them (a film either porous or slimy) in contact with the electrolyte and the other one (oxide film) in contact with Cu. At low frequency region ($f < 10$ Hz) the plateau of the $|Z|$ values with the phase angle approaching 0° is observed at lower frequencies than 0.1 Hz. $|Z|$ values tend to increase (6 hours) and subsequently their values decrease until the end of the test. This may be associated with a continuous dissolution process of the protective surface layers. These results also were consistent with the Nyquist diagram (not shown), where it could be observed that the data described a depressed, capacitive-like semicircle, with its center at the real axis, indicating that the corrosion process is under charge transfer control from the metal surface to the solution through the double electrochemical layer, and, as time elapsed,

the semicircle diameter increased but after 6 hours the semicircle diameter decreased constantly. This behavior is consistent with that observed in LPR measurements. Studies in 0.5 M H_2SO_4 solution show that the Nyquist plot comprises two capacitive semicircular arcs at low and high frequency regions, corresponding to two time constants. High and low frequency loops are attributed to charge transfer resistance for electrical double layer relaxation and diffusion mass transport of Cu ions from the surface, respectively, and the depressed nature of the capacitive semicircle is typical for solid metal electrodes that show frequency dispersion of the impedance data [35]. In this case, it is possible that due to the higher acid concentration the corrosion process is increased, and instead to observe two distinct time constants apparently only one is observed. This time constant corresponds to overlapping processes of charge transfer and diffusion.

Although copper is a relatively noble metal, it reacts easily in ordinary, oxygen-containing electrolytes. Corrosion behavior of copper in acidic, neutral, and alkaline solutions has been studied, and in all cases the dissolution of copper is balanced by oxygen reduction. Corrosion rate of copper is influenced by the pH and has its lowest value in slightly alkaline solutions. Stable oxides of copper can be formed reversibly in the pH range 8–12, and at pH values below 7, the dissolution of copper becomes significant, especially below pH 4-5, where the formation of stable surface oxides is not possible. The growth of copper(I) oxide takes place in a range of pH values above 4, and the film thickness decreases rapidly with pH decreasing below 4. Copper dissolution is controlled mainly by diffusion in the solution phase, in solutions of pH below 4, but with increasing pH, the formation of cubic Cu_2O oxide crystals is favored. This results in a change in dissolution control from mixed diffusion in oxide film, in solutions at pH 4-5, to diffusion in oxide film at pH > 6 [44].

However, because the concentration of Cu^+ at the metallic surface is much higher than Cu^{2+} [45], Cu dissolves through a monovalent species associated with anions. The initial step of the copper dissolution process is a charge transfer reaction resulting in formation of an adsorbed Cu^+ species [46]:

$$\mathrm{Cu} \longrightarrow \mathrm{Cu}^{+}_{\mathrm{ads}} + \mathrm{e}^{-} \tag{6}$$

The adsorbed Cu^+ species associates with an anion X^{n-} (hydroxyl or sulfate), which diffuses from the bulk solution onto electrode surface [47]:

$$\mathrm{X}^{n-}_{\mathrm{bulk}} \longrightarrow \mathrm{X}^{n-}_{\mathrm{surf}} \tag{7}$$

$$n\mathrm{Cu}^{+}_{\mathrm{ads}} + \mathrm{X}^{n-}_{\mathrm{surf}} \longrightarrow \left[\left(\mathrm{Cu}^{+}\right)\mathrm{X}^{n-}\right]_{\mathrm{surf}} \tag{8}$$

Then the complex species diffuses into the bulk solution:

$$\left[\left(\mathrm{Cu}^{+}\right)\mathrm{X}^{n-}\right]_{\mathrm{surf}} \longrightarrow \left[\left(\mathrm{Cu}^{+}\right)\mathrm{X}^{n-}\right]_{\mathrm{bulk}} \tag{9}$$

Increase in corrosion rate is owing to the increased diffusion rate of the complex species. Thus, only sulfate anions can be thought of to be the species which increases the corrosion rate of copper.

Generally, except under high cathodic overpotentials, copper does not displace hydrogen, and the presence of dissolved oxygen is essential for its cathodic reduction [46, 48]. Therefore the cathodic reaction is the reduction of oxygen which diffuses from the bulk solution and adsorbs onto the electrode surface [47]:

$$\mathrm{O}_{2,\,\mathrm{bulk}} \longrightarrow \mathrm{O}_{2,\,\mathrm{surf}} \tag{10}$$

$$\mathrm{O}_{2,\,\mathrm{surf}} \longrightarrow 2\mathrm{O}_{\mathrm{ads}} \tag{11}$$

$$\mathrm{O}_{\mathrm{ads}} + 2\mathrm{H}^{+} + 2\mathrm{e}^{-} \longrightarrow \mathrm{H}_2\mathrm{O} \tag{12}$$

This suggests that the time constant observed in high-middle frequency can be a hydroxyl or sulfate derivative of Cu which is adhered to the metallic surface, and the time constant at low frequencies corresponds either to the metallic surface or a thin film of copper oxides.

Figure 12(b) shows the superficial aspect of Cu after the corrosion test in 1.0 M H_2SO_4 solution at 25°C. The Cu surface did not show a significant attack, but it is observed that the lines generated by the grinding process are thinner than those observed on the surface of nickel. This suggests that the Cu corrosion process was higher than that of Ni. The superficial attack undergone by the Cu corresponds to that defined as uniform corrosion.

Figure 7 shows the Bode plot for Al. At higher frequency region ($f > 1000$ Hz), the plateau of the $|Z|$ values with the phase angle approaching 0° is observed at frequencies higher than 60 kHz, as time elapse. Again, this could be due to the presence of a film either porous or slimy onto Al surface. In the middle frequency region (1000 to 10 Hz), a maximum in the phase angle around 800 Hz is observed. It is observed that as time elapses the width of the phase angle spectrum is shifted to the high frequency region; that is, the width of the spectrum is located from the middle frequency region to the high frequency region. This suggests either the formation of a slimy film or a porous oxide onto the metal surface. In the first three hours of immersion, the maximum phase angle increases from 75° to 80° and remained virtually constant during the rest of the test. This is associated with an abrupt increase in the slope of the relationship log f-$|Z|$. The high-middle frequencies time constant could be assigned to the charge transfer of the corrosion process and to the formation of a protective layer. Prabhu and Rao [49] indicated that the corrosion process of aluminum includes the formation of Al^+ ions at the metal/oxide interface and their migration through the oxide/solution interface where they are oxidized to Al^{3+}, and, at the oxide/solution interface, OH^- or O^{2-} ions are also formed. The fact that all the three processes are represented by only one time constant could be attributed either to the overlapping of the loops of processes or to the assumption that one process only dominates and, therefore, excludes the other processes. The other explanation offered to the high frequency capacitive loop is the oxide film itself. At low frequency region ($f < 10$ Hz) the plateau of the $|Z|$ values with the phase angle approaching 0° is not observed. The apparent presence of a new time constant is observed. However, from Nyquist plot (not shown), a large capacitive semicircle at high-middle frequencies and an inductive loop at low frequencies were observed. The capacitive semicircle at high-middle frequencies characterizes the active state of

the interface when the Al is exposed to the sulfuric acid solution and it is related to the charge transfer of the corrosion process and the double layer behavior, and the inductive loop observed is attributed to the adsorption of species which promotes the corrosion rate [50]. In this case, the inductive loop may be related to the relaxation process obtained by adsorption and incorporation of ions and charged intermediates onto and into the oxide film [34, 49]. Behavior described from EIS measurements is consistent with that observed in LPR measurements.

In acid solution the mechanism of dissolution of aluminum is as follows [49]:

$$\mathrm{Al} + \mathrm{H_2O} \longrightarrow \mathrm{AlOH_{ads}} + \mathrm{H^+} + \mathrm{e^-} \quad (13)$$

$$\mathrm{AlOH_{ads}} + 5\mathrm{H_2O} + \mathrm{H^+} \longrightarrow \mathrm{Al^{3+}} + 6\mathrm{H_2O} + 2\mathrm{e^-} \quad (14)$$

$$\mathrm{Al^{3+}} + \mathrm{H_2O} \longrightarrow [\mathrm{AlOH}]^{2+} + \mathrm{H^+} \quad (15)$$

$$[\mathrm{AlOH}]^{2+} + \mathrm{X^-} \longrightarrow [\mathrm{AlOHX}]^{+} \quad (16)$$

Thus soluble complex ion formed leads to the dissolution of the metal. The major cathodic reaction is evolution of hydrogen gas according to the following steps:

$$\mathrm{H^+} + \mathrm{e^-} \longrightarrow \mathrm{H_{ads}} \quad (17)$$

$$\mathrm{H_{ads}} + \mathrm{H_{ads}} \longrightarrow \mathrm{H_2} \quad (18)$$

This suggests that the time constant observed characterizes the active state of the Al surface and the inductive loop is related to the relaxation process due to the adsorption and incorporation of ions and charged intermediates onto and into the oxide film.

Figure 12(c) shows the superficial aspect of Al after the corrosion test in 1.0 M H_2SO_4 solution at 25°C. It is observed that the Al surface shows a severe attack. The presence of pitting attack and corrosion through grain boundaries are observed. Clearly aluminum was unable to develop a protective oxide.

Figure 8 shows the Bode plot for Ni_3Al. The impedance spectrum is very similar to the Ni, though some differences are observed. At higher frequency region ($f > 1000$ Hz), the plateau of the $|Z|$ values with the phase angle approaching 0° is observed at frequencies higher than 30 kHz. This could be due to the presence of a film either porous or slimy onto Ni_3Al surface. In the middle frequency region (1000 to 10 Hz), a maximum in the phase angle is observed, but the shape of the phase angle spectrum is not according to a Gaussian distribution; that is, the width of the phase angle spectrum is located from the high frequency region to the low frequency region, suggesting the presence of two time constants. Maximum phase angle decreases after 3 hours from 81° to 76°. However the slope of the relationship log f-$|Z|$ remains practically constant. A constant slope and a wider spectrum may be due to the presence of a protective slimy film strongly adhered to the metallic surface. At low frequency region ($f <$ 10 Hz) the plateau of the $|Z|$ values with the phase angle approaching 0° is not clearly observed; instead an apparent plateau is observed. From Nyquist diagram (not shown) a contraction of Z_{real} was observed; that is, there is a relationship between the apparent plateau and the contraction of capacitive loop at low frequencies. Some authors suggest that the contraction of the capacitive loop is due to the presence of processes controlled by mass-transfer [51, 52], where this sort of mass-transfer processes can show three different diffusion characters [53]: the first one is called semi-infinite diffusion process and it happens when the thickness of stagnant layer is infinite (Warburg diffusion), the second one happens when the thickness of the stagnant layer is finite and there is a contraction of the real part and it is called transmissive finite diffusion process, and the third one happens when only the transmission takes place in a limited distance and it is called reflective finite diffusion process. Therefore, it can be considered that there is a transmissive finite diffusion process due to the presence of a slimy film strongly adhered to the metallic surface. It is observed that the $|Z|$ values tend to increase (18 hours) and subsequently their values fluctuate until the end of the test. The initial behavior may be due to the presence of the viscous layer which limited the charge transfer processes, and subsequently its dissolution or its detachment resulted in the observed fluctuations. This behavior is consistent with that observed in LPR measurements.

It is known that the high corrosion resistance of the intermetallic compounds of Ni_3Al type is due to its ability to develop a protective passive film with a high chemical stability (Al_2O_3) [54]. Therefore its performance depends on its ability to develop a continuous and stable film of Al_2O_3. Accordingly, the main anodic and cathodic reactions are those described above (reactions (13)–(18)).

Figure 13(a) shows the superficial aspect of Ni_3Al after the corrosion test in 1.0 M H_2SO_4 solution at 25°C. In general the characteristic microstructure of the Ni_3Al consists of two phases where the matrix corresponds to γ_{Ni}-$\gamma'_{\mathrm{Ni_3Al}}$ and the dendritic phase to β_{NiAl}-$\gamma'_{\mathrm{Ni_3Al}}$ [55, 56]. This type of microstructure is characteristic of intermetallic Ni_3Al and its formation is attributed to the difference between the melting points of the constituent phases. From figure, it is possible to observe that the Ni_3Al base alloy showed only localized attack (dissolution) in dendritic phases, that is, the phases with the higher aluminum content. It is considered that this localized attack is the reason for the fluctuations observed in measurements of i_{corr} (Figure 4). Once the dendritic phases were dissolved i_{corr} values remain stable. The matrix phase of the intermetallic alloy did not show a significant attack; it only showed the presence of lines generated by the grinding process. This kind of preferential dissolution is observed due to the formation of microgalvanic cells, where the matrix phase acted as cathode and the dendritic phase as anode. In the presence of two phases where one of the phases has either different chemical composition or microstructure, one of these phases will act as cathode and the other as an active anode; this will cause the preferential dissolution of one of the phases, the one which acts as active anode, inducing preferential, localized dissolution within the alloy [28]. These results indicate that the presence of the β phase is chemically less stable.

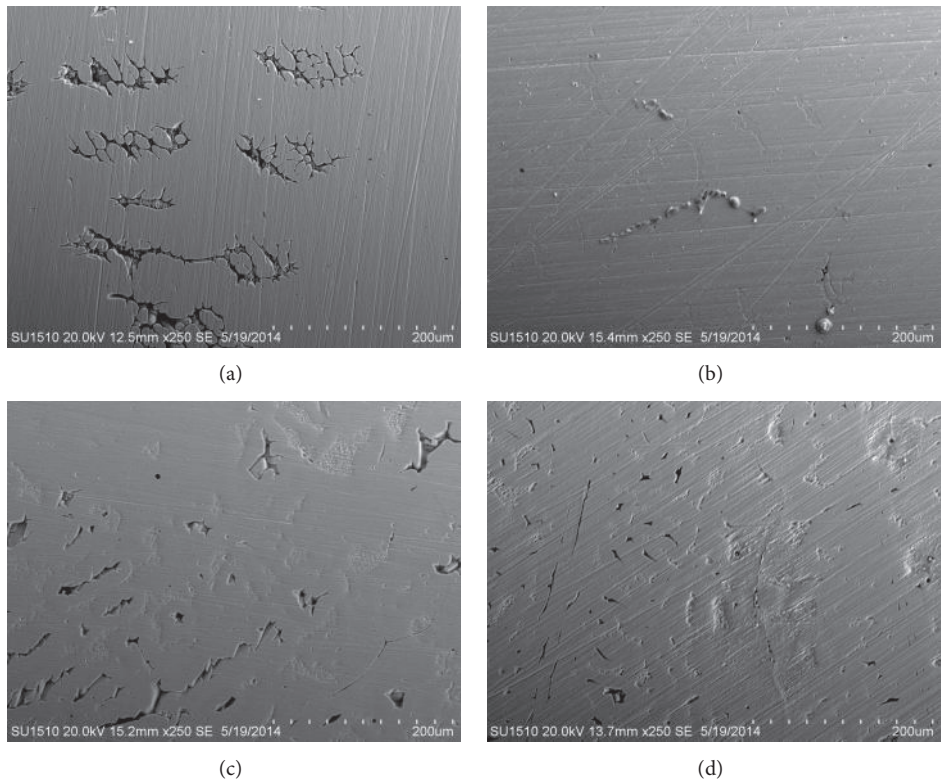

FIGURE 13: Micrograph of the corroded surfaces of (a) Ni_3Al, (b) Ni_3Al-1Cu, (c) Ni_3Al-3Cu, and (d) Ni_3Al-3Cu in 1.0 M H_2SO_4 solution at 25°C.

Figure 9, Bode plot for Ni_3Al-1Cu, shows that the Cu addition modified the electrochemical behavior of the Ni_3Al-base alloy. At higher frequency region ($f > 1000$ Hz) the behavior was similar. In the middle frequency region (1000 to 10 Hz), a maximum in the phase angle is observed, but the phase angle spectrum is wider and the presence of a second time constant is evident. A slight increase in the phase angle (74° to 77°) and also a slight increase in the slope of the relationship log f-$|Z|$ are observed. A constant slope and a wider spectrum may be due to the presence of a protective slimy film strongly adhered to the metallic surface. This is associated with the observed behavior at low frequency region ($f <$ 10 Hz) where a plateau is well defined, and the $|Z|$ values increase as time evolves. However, from Nyquist diagram (not shown), a slight contraction of Z_{real} was observed. This indicates that there are still processes controlled by mass-transfer. It has been suggested that the suppression of the low frequency inductive loop from the impedance spectra of the Cu-containing austenite and ferrite implies inhibition of the mass transfer process due to the presence of Cu [37].

Figure 13(b) shows the superficial aspect of Ni_3Al-1Cu after the corrosion test in 1.0 M H_2SO_4 solution at 25°C. From figure it is possible to observe that the addition of Cu led to an increase in the ratio γ-γ'/β due to the reduction in the number and volume of the dendritic phases. This indicates that the amount of β-phase into dendrites is less, and therefore the Ni_3Al-1Cu alloy only showed slight localized attack (dissolution) in dendritic phases. Again, the matrix phase did not show a significant attack.

Figure 10 shows the Bode plot for Ni_3Al-3Cu. The main differences are observed at the middle and low frequency regions. In the middle frequency region (1000 to 10 Hz), a maximum in the phase angle is observed; the width of the phase angle spectrum is located from the high frequency region to the low frequency region. Maximum phase angle increases after 3 hours from 76° to 79°, but after that a decrease is observed (76° to 74°). The slope of the relationship log f-$|Z|$ increases after 3 hours and then decreases as time evolves. At low frequency region ($f <$ 10 Hz) an apparent plateau is observed. From Nyquist diagram (not shown) a contraction of Z_{real} was observed. This indicates that there are processes controlled by mass-transfer. The behavior observed is consistent with the LPR measurements.

Figure 13(c) shows the superficial aspect of Ni_3Al-3Cu after the corrosion test in 1.0 M H_2SO_4 solution at 25°C. From figure it is possible to observe the presence of three phases, the matrix (γ-γ') and two dendritic phases. The corrosion attack in the dendritic phases was different. It may be inferred that the main difference between the dendritic phases is the proportion of the β-phase. The dendrites with a higher content of β-phase showed a greater attack than those dendrites with lower β-phase content. The matrix phase did not show a significant attack.

Figure 11 shows the Bode plot for Ni_3Al-5Cu. The main differences are observed at the middle and low frequency regions. In the middle frequency region (1000 to 10 Hz), a maximum in the phase angle is observed, but width of the phase angle spectrum is located from the high frequency

region to the lower frequency region. As time evolves, the maximum phase angle decreases from 78° to 74°. The slope of the relationship log f-$|Z|$ steadily decreases as time passes. At low frequency region ($f < 10$ Hz) the plateau of the $|Z|$ values is not clearly observed, instead an apparent plateau is observed. From Nyquist diagram (not shown) a contraction of Z_{real} was observed, like an inductive loop. This indicates that there are processes controlled by mass-transfer. It is observed that the $|Z|$ values constantly decrease until the end of the test.

Figure 13(d) shows the superficial aspect of Ni_3Al-5Cu after the corrosion test in 1.0 M H_2SO_4 solution at 25°C. Again, from figure, the presence of three phases is observed, the matrix (γ-γ') and two dendritic phases. The proportion of dendrites with high β-phase content is less; however the dissolution of the dendrites with low β-phase content was greater than that observed in the Ni_3Al-1Cu (Figure 13(b)). The matrix phase did not show a significant attack.

3.5. Analysis of Impedance Data. In order to interpret the electrochemical behavior of a system from EIS spectra, an appropriate physical model of the electrochemical reactions occurring at the electrode surface is necessary. Interpretation of the electrochemical behavior of a system from EIS spectra requires an appropriate physical model of the electrochemical reactions into the electrode surface. In this sense, the equivalent circuits are used to model the electrochemical behavior and calculate the parameters of interest, such as electrolyte resistance (R_s), charge transfer resistance (R_{ct}), and double layer capacitance (C_{dl}). However, when a nonideal frequency response is present, it is accepted to employ distributed circuit elements in an equivalent circuit. The most widely used is the constant phase element (CPE). CPE is used in a model in place of a capacitor to compensate the inhomogeneity in the system which takes into account the irregularities of the surface such as roughness or because properties such as double layer capacitance and charge transfer rate are nonuniformly distributed. CPE is an element whose impedance value is a function of the frequency and whose phase is independent of the frequency and its impedance is defined as

$$Z_{\text{CPE}} = \frac{1}{Q\left(j\omega\right)^n}, \tag{19}$$

where Q is a proportional factor that indicates the combination of properties related to both the surfaces and electroactive species independent of frequency; j is imaginary number ($\sqrt{-1}$); ω is the angular frequency and equal to $2\pi f$, where f is the frequency; and n has the meaning of a phase shift and is related to a slope of the log $|Z|$ versus log f plots and usually is in the range 0.5 and 1. When the value of n is equal to 1, the CPE describes an ideal capacitor with Y_o equal to the capacitance. For $0.5 < n < 1$ the CPE describes a distribution of dielectric relaxation times in frequency space, and when n is equal to 0.5 the CPE represents a Warburg impedance with diffusional character. In these situations the semicircle in the Z_{re}-Z_{im} spectra is more and more depressed and the depression degree depends on the phase of the CPE [57].

For Ni and Cu, in the lower frequency region, the phase angle does not approach 0°, also from the Nyquist plot, in the lowest frequency region, the $-Z_{\text{img}}$ versus Z_{real} curves, a deviation from the Z_{real} axis or a contraction of the capacitive loop was observed. This is evidence that a diffusion process should be taken into account. Therefore the equivalent circuit model was constructed on that basis and it is given in Figure 14(a). As discussed previously, the impedance spectra indicate the presence of two time constants. The first time constant represents the surface layer (rich in metal hydroxides and/or metal sulfates) through which the metal ions diffuse. Q_f represents the CPE of the surface layer, R_f is the resistance of the ion conducting paths that developed in the surface layer, and W is the element for the finite length Warburg (FLW) diffusion:

$$Z_W = \frac{R_W * \tanh\left(\left[\sqrt{-1} * T * \omega\right]^P\right)}{\left(\sqrt{-1} * T * \omega\right)^P}. \tag{20}$$

FLW is the solution of the one-dimensional diffusion equation of a particle, where $T = L^2/D$ (L is the effective diffusion thickness, and D is the effective diffusion coefficient of the particle) and $P = 0.5$. This version of the Warburg element terminates in a finite resistance where at very low frequencies, Z_{re} approaches R_W and Z_{im} goes to zero.

The second time constant represents the charge-transfer process of metal dissolution or the oxide dissolution, where R_{ct} describes the charge-transfer resistance and Q_{dl} the constant phase element (CPE) relating to the double layer capacitor. Similar models have been employed for Cu (or its alloys) treated with different inhibitors [44, 58–60].

In order to model the Al impedance spectra (Figures 7 and 15(a)) different models were used. However, the equivalent circuit with the best fit is that shown in Figure 14(b). In this equivalent circuit of nine elements R_s is the solution resistance and R_{ct} is the charge transfer resistance, R_L and L represent the inductive elements, including a constant phase element in parallel with the series capacitors C_1, C_2 and series resistors R_1 and R_2 [49]. The polarization resistance R_p and double layer capacitance C_{dl} are calculated from

$$\begin{aligned} R_p &= R_L + R_{\text{ct}} + R_1 + R_2, \\ C_{\text{dl}} &= C_1 + C_2. \end{aligned} \tag{21}$$

Because the intermetallic alloys showed a big capacitive loop (Figure 15(b)), and the width of the phase angle spectrum is located from the high frequency region to the low frequency region, and also at lower frequency region, an apparent plateau and the contraction of capacitive loop were observed; the equivalent circuit used is shown in Figure 14(c). R_s is the solution resistance; R_{ct} and Q are the resistance and the CPE associated with the charge-transfer reaction, respectively. R_1 and L are the resistance and inductance related to the adsorption/desorption process, respectively. This equivalent circuit has been used when the complex plane plot presents one big capacitive loop and one inductive loop at low frequencies. The capacitive loop is associated with the double layer capacity and the inductive loop is associated with the adsorption/desorption processes [34]. For modeling the equivalent circuits, an error criterion of $\chi^2 \ll 10^{-4}$ was used.

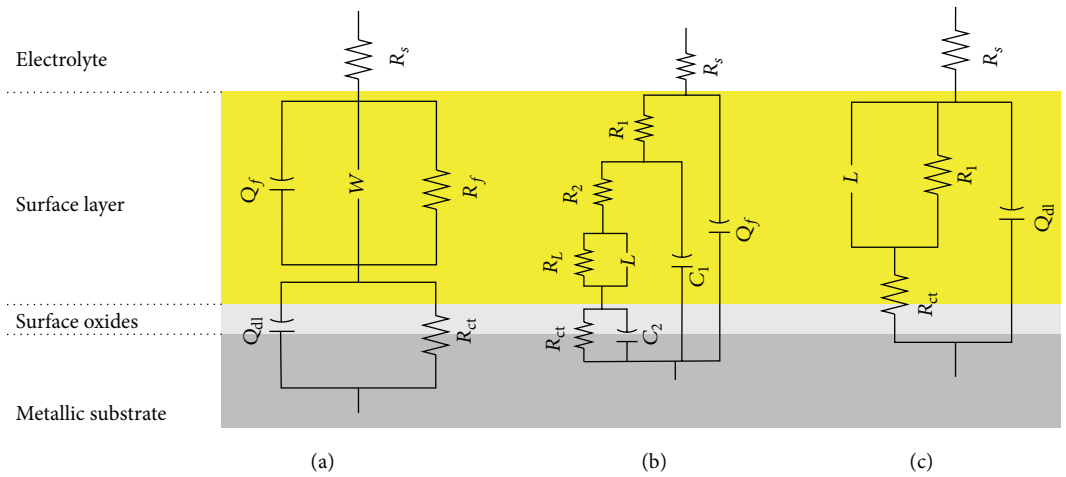

FIGURE 14: Equivalent circuits (a) for Ni, Cu; (b) for Al; and (c) for intermetallic alloys.

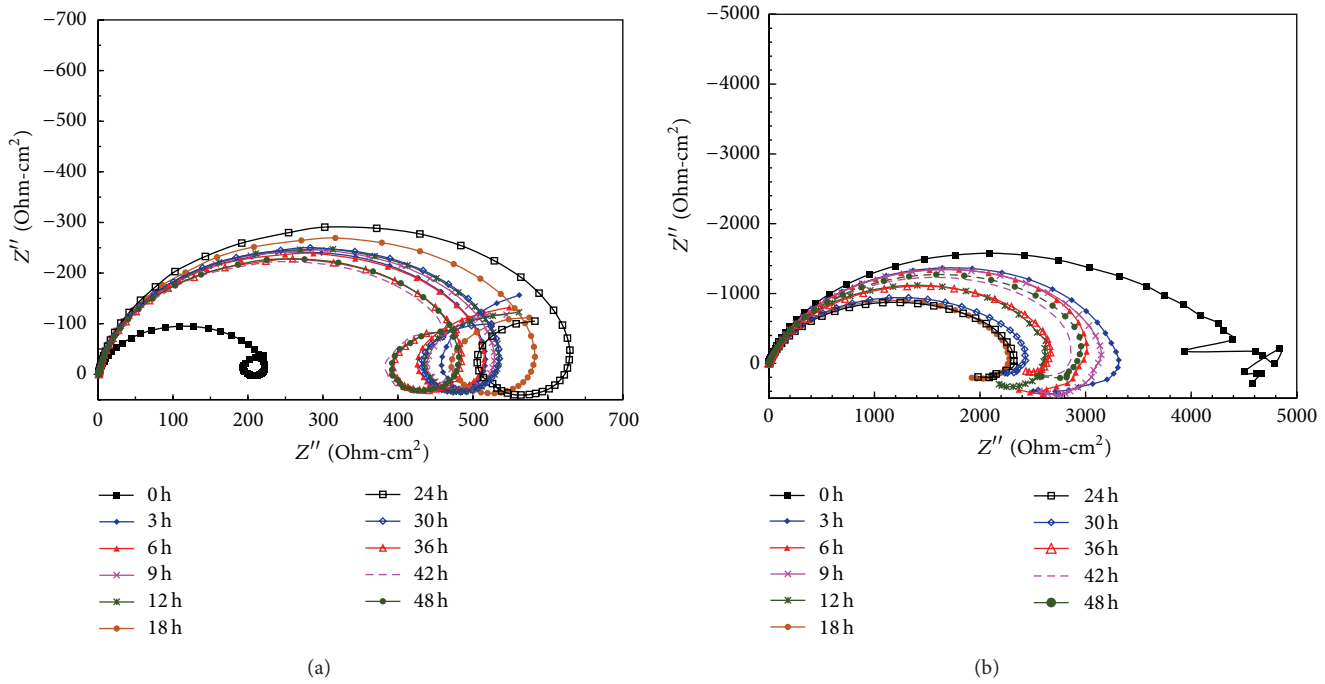

FIGURE 15: Examples of Nyquist plots for (a) Al; (b) Ni_3Al-5Cu.

From simulations R_{ct} values were obtained and compared with those of corrosion current measurements.

Figure 16 shows the variation of i_{corr} values versus time for the materials evaluated. i_{corr} values were obtained from R_{ct} values calculated for each simulated condition. The calculation of i_{corr} was realized using Stern-Geary expression (1) and the b_a and b_c values reported in Table 1. Comparing Figure 16 with Figure 4, the excellent agreement between the i_{corr} values calculated from the EIS measurements with those from LPR measurements is observed. This suggests that the equivalent circuits proposed are suitable to simulate the impedance spectra and are consistent with the surface processes previously described. EIS measurements confirm that the Ni_3Al-1Cu alloy showed the best performance and Al and Cu the worst performance. It is assumed that the worse performance of the Ni_3Al alloys with higher content of Cu was due to the presence of dendrites with different content of β-phase.

4. Conclusions

Effect of Cu addition on the corrosion behavior of Ni_3Al and pure elements (Cu, Ni, and Al) in 1.0 M H_2SO_4 solution was studied by electrochemical measurements. Results indicate the following: polarization curves for intermetallic alloys (Ni_3Al, Ni_3Al-xCu) showed an active-passive behavior with a wide passivation zone, OCP measurements indicate that the Cu addition influences the kinetics of the anodic reaction by

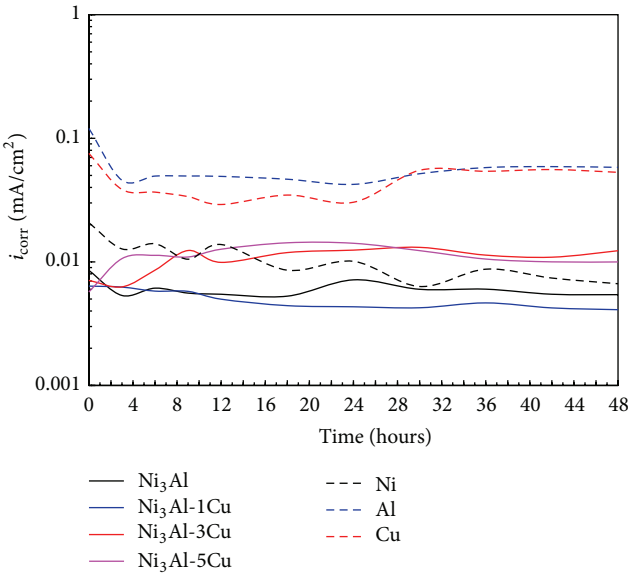

FIGURE 16: I_{corr} variation against time for the tested materials. Determined from the R_{ct} values of EIS measurements.

shifting the E_{corr} values toward nobler values, and from LPR measurements it is observed that the addition of 1% Cu to the Ni_3Al alloy reduces the corrosion rate of the base alloy; however, the additions of 3% and 5% Cu increase slight the corrosion rate. EIS results agree with LPR measurements. In general, impedance spectra obtained are determined by two time constants, which may be associated with the presence of two protective layers, one of them (a film either porous or slimy, relating to the mass transport) in contact with the electrolyte and the other one (oxide film, relating to the charge transfer process) in contact with the metallic surface. The equivalence circuit parameters obtained show an excellent agreement between the i_{corr} values calculated from the EIS measurements and those from LPR measurements, suggesting that the equivalent circuits proposed are suitable to simulate the impedance spectra and are consistent with the surface processes described. SEM analysis shows that Cu addition reduces the presence of dendritic phases and that the degradation process of the intermetallic alloys was caused by localized attack (dissolution) of the dendritic phases; this is due to the formation of microgalvanic cells, where the matrix phase acted as cathode and the dendritic phase as anode.

Conflict of Interests

The authors declare that there is no conflict of interests regarding the publication of this paper.

Acknowledgments

Financial support from Consejo Nacional de Ciencia y Tecnología (CONACYT, Mexico) (Projects nos. 159913, 159898, and 198687) is gratefully acknowledged.

References

[1] Q. B. Zhang and Y. X. Hua, "Corrosion inhibition of mild steel by alkylimidazolium ionic liquids in hydrochloric acid," *Electrochimica Acta*, vol. 54, no. 6, pp. 1881–1887, 2009.

[2] N. D. Greene, C. R. Bishop, and M. Stern, "Corrosion and electrochemical behavior of chromium-noble metal alloys," *Journal of the Electrochemical Society*, vol. 108, no. 9, pp. 836–841, 1961.

[3] J. Guo, M. Seo, Y. Sato, G. Hultquist, C. Leygraf, and N. Sato, "Electrochemical behavior and surface composition of copper containing ferritic stainless steel in sulfuric acid solution," *Corrosion Engineering*, vol. 35, pp. 283–288, 1986.

[4] A. Higginson, R. C. Newman, and R. P. M. Procter, "The passivation of Fe-Cr-Ru alloys in acidic solutions," *Corrosion Science*, vol. 29, no. 11-12, pp. 1293–1318, 1989.

[5] A. A. Hermas, K. Ogura, and T. Adachi, "Accumulation of copper layer on a surface in the anodic polarization of stainless steel containing Cu at different temperatures," *Electrochimica Acta*, vol. 40, no. 7, pp. 837–844, 1995.

[6] C. Kato, H. J. Grabke, B. Egert, and G. Panzner, "Electrochemical and surface analytical studies on hydrogen permeation with Fe-Cu alloys in sulfuric acid with and without H_2S," *Corrosion Science*, vol. 24, no. 7, pp. 591–611, 1984.

[7] M. Abdallah, "Guar gum as corrosion inhibitor for carbon steel in sulfuric acid solutions," *Portugaliae Electrochimica Acta*, vol. 22, no. 2, pp. 161–175, 2004.

[8] E. P. Busso and F. A. McClintock, "Mechanisms of cyclic deformation of NiAl single crystals at high temperatures," *Acta Metallurgica et Materialia*, vol. 42, no. 10, pp. 3263–3275, 1994.

[9] R. Jayaram and M. K. Miller, "An atom probe study of grain boundary and matrix chemistry in microalloyed NiAl," *Acta Metallurgica et Materialia*, vol. 42, no. 5, pp. 1561–1572, 1994.

[10] R. D. Noebe, R. R. Bowman, and M. V. Nathal, "Physical and mechanical properties of the B2 compound NiAl," *International Materials Reviews*, vol. 38, no. 4, pp. 193–232, 1993.

[11] D. B. Miracle, "The physical and mechanical properties of NiAl," *Acta Metallurgica et Materialia*, vol. 41, pp. 649–684, 1993.

[12] J. Colin, C. Gonzalez, R. Herrera, and J. A. Juarez-Islas, "Analysis of chill-cast NiAl intermetallic compound with copper additions," *Journal of Materials Engineering and Performance*, vol. 11, no. 5, pp. 487–491, 2002.

[13] A. Chiba, S. Hanada, and S. Watanabe, "Improvement in ductility of Ni_3Al by γ former doping," *Materials Science and Engineering A*, vol. 152, no. 1-2, pp. 108–113, 1992.

[14] K. Ishida, R. Kainuma, N. Ueno, and T. Nishizawa, "Ductility enhancement in NiAl (B2)-base alloys by microstructural control," *Metallurgical Transactions A*, vol. 22, no. 2, pp. 441–446, 1991.

[15] C.-H. Tsau, "Rapid solidification effect on the Ni-25Al-xFe intermetallics," *Intermetallics*, vol. 9, no. 12, pp. 1085–1087, 2001.

[16] N. S. Stoloff, C. T. Liu, and S. C. Deevi, "Emerging applications of intermetallics," *Intermetallics*, vol. 8, no. 9-11, pp. 1313–1320, 2000.

[17] V. K. Sikka, S. C. Deevi, S. Viswanathan, R. W. Swindeman, and M. L. Santella, "Advances in processing of Ni_3Al-based intermetallics and applications," *Intermetallics*, vol. 8, no. 9–11, pp. 1329–1337, 2000.

[18] K. Morsi, "Review: reaction synthesis processing of Ni-Al intermetallic materials," *Materials Science and Engineering A*, vol. 299, no. 1-2, pp. 1–15, 2001.

[19] F. Scheppe, P. R. Sahm, W. Hermann, U. Paul, and J. Preuhs, "Nickel aluminides: a step toward industrial application," *Materials Science and Engineering A*, vol. 329–331, pp. 596–601, 2002.

[20] P. F. Tortorelli and K. Natesan, "Critical factors affecting the high-temperature corrosion performance of iron aluminides," *Materials Science and Engineering A*, vol. 258, no. 1-2, pp. 115–125, 1998.

[21] J. G. Gonzalez-Rodriguez, E. Mejia, M. A. Lucio-Garcia, V. M. Salinas-Bravo, J. Porcayo-Calderon, and A. Martinez-Villafañe, "An electrochemical study of the effect of Li on the corrosion behavior of Ni_3Al intermetallic alloy in molten (Li + K) carbonate," *Corrosion Science*, vol. 51, no. 8, pp. 1619–1627, 2009.

[22] M. C. García-Alonso, M. F. Lopez, M. L. Escudero, J. L. González-Carrasco, and D. G. Morris, "Corrosion behaviour of an Fe_3Al-type intermetallic in a chloride containing solution," *Intermetallics*, vol. 7, no. 2, pp. 185–191, 1999.

[23] C. D. Arrieta-Gonzalez, J. Porcayo-Calderon, V. M. Salinas-Bravo, J. G. Gonzalez-Rodriguez, and J. G. Chacon-Nava, "Electrochemical behavior of Fe_3Al modified with Ni in Hank's solution," *International Journal of Electrochemical Science*, vol. 6, no. 9, pp. 4016–4031, 2011.

[24] J. Porcayo-Calderon, L. M. M. de la Escalera, J. Canto, M. Casales-Diaz, and V. M. Salinas-Bravo, "Effect of the temperature on the CO_2-corrosion of Ni_3Al," *International Journal of Electrochemical Science*, vol. 10, pp. 3136–3151, 2015.

[25] C. L. Zeng, P. Y. Guo, and W. T. Wu, "Electrochemical impedance spectra for the corrosion of two-phase Cu–15Al alloy in eutectic (Li, K)$_2CO_3$ at 650 °C in air," *Electrochimica Acta*, vol. 49, no. 9-10, pp. 1445–1450, 2004.

[26] W. H. Lee and R. Y. Lin, "Hot corrosion mechanism of intermetallic compound Ni_3Al," *Materials Chemistry and Physics*, vol. 77, no. 1, pp. 86–96, 2003.

[27] M. Stern and A. L. Geary, "Electrochemical polarization. I. A theoretical analysis of the shape of polarization curves," *Journal of the Electrochemical Society*, vol. 104, no. 1, pp. 56–63, 1957.

[28] J. G. González-Rodriguez, J. C. Colín, S. Serna, B. Campillo, and J. L. Albarran, "Effect of macroalloying with Cu on the corrosion resistance of rapidly solidified NiAl intermetallic in 0.5 M H_2SO_4," *Materials Science and Engineering A*, vol. 448, no. 1-2, pp. 158–164, 2007.

[29] A. Pardo, M. C. Merino, A. E. Coy, R. Arrabal, F. Viejo, and A. M'hich, "Corrosion behaviour of AISI 304 stainless steel with Cu coatings in H_2SO_4," *Applied Surface Science*, vol. 253, no. 23, pp. 9164–9176, 2007.

[30] G. Moretti and F. Guidi, "Tryptophan as copper corrosion inhibitor in 0.5 M aerated sulfuric acid," *Corrosion Science*, vol. 44, no. 9, pp. 1995–2011, 2002.

[31] J. M. Bastidas, P. Pinilla, E. Cano, J. L. Polo, and S. Miguel, "Copper corrosion inhibition by triphenylmethane derivatives in sulphuric acid media," *Corrosion Science*, vol. 45, no. 2, pp. 427–449, 2003.

[32] D. Tromans and T. Ahmed, "Active/passive behavior of copper in strong sulfuric acid," *Journal of the Electrochemical Society*, vol. 145, no. 2, pp. 601–608, 1998.

[33] A. H. Moreira, A. V. Benedetti, P. L. Cabot, and P. T. A. Sumodjo, "Electrochemical behaviour of copper electrode in concentrated sulfuric acid solutions," *Electrochimica Acta*, vol. 38, no. 7, pp. 981–987, 1993.

[34] M. R. F. Hurtado, P. T. A. Sumodjo, and A. V. Benedetti, "Electrochemical studies with a Cu-5wt.%Ni alloy in 0.5 M H_2SO_4," *Electrochimica Acta*, vol. 48, no. 19, pp. 2791–2798, 2003.

[35] I. O. Arukalam, I. C. Madufor, O. Ogbobe, and E. E. Oguzie, "Acidic corrosion inhibition of copper by hydroxyethyl cellulose," *The British Journal of Applied Science & Technology*, vol. 4, no. 9, pp. 1445–1460, 2014.

[36] M. A. Amin, H. Shokry, and E. M. Mabrouk, "Nickel corrosion inhibition in sulfuric acid-Electrochemical studies, morphologies, and theoretical approach," *Corrosion*, vol. 68, no. 8, pp. 699–712, 2012.

[37] E. E. Oguzie, J. Li, Y. Liu et al., "The effect of Cu addition on the electrochemical corrosion and passivation behavior of stainless steels," *Electrochimica Acta*, vol. 55, no. 17, pp. 5028–5035, 2010.

[38] J. R. Vilche and A. J. Arvía, "Kinetics and mechanism of the nickel electrode-I. Acid solutions containing a high concentration of chloride and nickel ions," *Corrosion Science*, vol. 15, no. 6–12, pp. 419–431, 1975.

[39] R. S. Gonçalves, D. S. Azambuja, and A. M. S. Lucho, "Electrochemical studies of propargyl alcohol as corrosion inhibitor for nickel, copper, and copper/nickel (55/45) alloy," *Corrosion Science*, vol. 44, no. 3, pp. 467–479, 2002.

[40] V. Freger and S. Bason, "Characterization of ion transport in thin films using electrochemical impedance spectroscopy: I. Principles and theory," *Journal of Membrane Science*, vol. 302, no. 1-2, pp. 1–9, 2007.

[41] J. E. G. González and J. C. Mirza-Rosca, "Study of the corrosion behavior of titanium and some of its alloys for biomedical and dental implant applications," *Journal of Electroanalytical Chemistry*, vol. 471, no. 2, pp. 109–115, 1999.

[42] S. Tamilselvi, V. Raman, and N. Rajendran, "Corrosion behaviour of Ti-6Al-7Nb and Ti-6Al-4V ELI alloys in the simulated body fluid solution by electrochemical impedance spectroscopy," *Electrochimica Acta*, vol. 52, no. 3, pp. 839–846, 2006.

[43] F. Matemadombo and T. Nyokong, "Characterization of self-assembled monolayers of iron and cobalt octaalkylthiosubstituted phthalocyanines and their use in nitrite electrocatalytic oxidation," *Electrochimica Acta*, vol. 52, no. 24, pp. 6856–6864, 2007.

[44] M. Metikoš-Huković, R. Babić, and I. Paić, "Copper corrosion at various pH values with and without the inhibitor," *Journal of Applied Electrochemistry*, vol. 30, no. 5, pp. 617–624, 2000.

[45] K. N. Oh, I. H. Toor, S. H. Ahn, and H. S. Kwon, "Effects of Cu on the passive film stability of Fe–20Cr–xCu (x = 0, 2, 4 wt.%) alloys in H_2SO_4 solution," *Electrochimica Acta*, vol. 88, pp. 170–176, 2013.

[46] E. Mattsson and J. O. M. Bockris, "Galvanostatic studies of the kinetics of deposition and dissolution in the copper + copper sulphate system," *Transactions of the Faraday Society*, vol. 55, pp. 1586–1601, 1959.

[47] S. Magaino, "Corrosion rate of copper rotating-disk-electrode in simulated acid rain," *Electrochimica Acta*, vol. 42, no. 3, pp. 377–382, 1997.

[48] Y. Lu, H. Xu, J. Wang, and X. Kong, "Oxygen reduction mechanism on copper in a 0.5 M H_2SO_4," *Electrochimica Acta*, vol. 54, no. 15, pp. 3972–3978, 2009.

[49] D. Prabhu and P. Rao, "*Garcinia indica* as an environmentally safe corrosion inhibitor for aluminium in 0.5 M phosphoric acid," *International Journal of Corrosion*, vol. 2013, Article ID 945143, 11 pages, 2013.

[50] J. H. Hong, S. H. Lee, J. G. Kim, and J. B. Yoon, "Corrosion behaviour of copper containing low alloy steels in sulphuric acid," *Corrosion Science*, vol. 54, no. 1, pp. 174–182, 2012.

[51] Y. Li, D. Zhang, and J. Wu, "Study on kinetics of cathodic reduction of dissolved oxygen in 3.5% sodium chloride solution," *Journal of Ocean University of China*, vol. 9, no. 3, pp. 239–243, 2010.

[52] L. M. Rivera-Grau, M. Casales, I. Regla et al., "Effect of organic corrosion inhibitors on the corrosion performance of 1018 carbon steel in 3% NaCl solution," *International Journal of Electrochemical Science*, vol. 8, no. 2, pp. 2491–2503, 2013.

[53] F. Kuang, D. Zhang, Y. Li, Y. Wan, and B. Hou, "Electrochemical impedance spectroscopy analysis for oxygen reduction reaction in 3.5% NaCl solution," *Journal of Solid State Electrochemistry*, vol. 13, no. 3, pp. 385–390, 2009.

[54] P. F. Tortorelli and K. Natesan, "Critical factors affecting the high-temperature corrosion performance of iron aluminides," *Materials Science and Engineering A*, vol. 258, no. 1-2, pp. 115–125, 1998.

[55] O. Hunziker and W. Kurz, "Directional solidification and phase equilibria in the Ni-Al system," *Metallurgical and Materials Transactions A: Physical Metallurgy and Materials Science*, vol. 30, no. 12, pp. 3167–3175, 1999.

[56] G. Rosas, R. Esparza, A. Bedolla, O. Flores, and R. Perez, "Effect of Li alloying on the microstructure and mechanical properties of Ni_3Al," *Advances in Technology of Materials and Materials Processing*, vol. 9, pp. 99–102, 2007.

[57] J. E. Ferrer and L. Victori, "Oxygen evolution reaction on the iridium electrode in basic medium studied by electrochemical impedance spectroscopy," *Electrochimica Acta*, vol. 39, no. 4, pp. 581–588, 1994.

[58] M. Metikoš-Huković, R. Babić, and A. Marinović, "Spectrochemical characterization of benzotriazole on copper," *Journal of the Electrochemical Society*, vol. 145, no. 12, pp. 4045–4051, 1998.

[59] J. Hayon, C. Yarnitzky, J. Yahalom, and A. Bettelheim, "Surface processes characterization for the corrosion of copper in borate solutions: I. The effect of sodium dodecylsulfate," *Journal of the Electrochemical Society*, vol. 149, no. 7, pp. B314–B320, 2002.

[60] M. Finšgar, "2-Mercaptobenzimidazole as a copper corrosion inhibitor: part I. Long-term immersion, 3D-profilometry, and electrochemistry," *Corrosion Science*, vol. 72, pp. 82–89, 2013.